



2018

ELUCIDATING THE ROLE OF NIDOGEN IN THE FUSION OF THE CHOROID FISSURE

Nicholas W. Carrara

University of Kentucky, nicholas.carrara@uky.edu

Digital Object Identifier: <https://doi.org/10.13023/etd.2018.362>

[Right click to open a feedback form in a new tab to let us know how this document benefits you.](#)

Recommended Citation

Carrara, Nicholas W., "ELUCIDATING THE ROLE OF NIDOGEN IN THE FUSION OF THE CHOROID FISSURE" (2018). *Theses and Dissertations--Biology*. 54.
https://uknowledge.uky.edu/biology_etds/54

This Master's Thesis is brought to you for free and open access by the Biology at UKnowledge. It has been accepted for inclusion in Theses and Dissertations--Biology by an authorized administrator of UKnowledge. For more information, please contact UKnowledge@lsv.uky.edu.

STUDENT AGREEMENT:

I represent that my thesis or dissertation and abstract are my original work. Proper attribution has been given to all outside sources. I understand that I am solely responsible for obtaining any needed copyright permissions. I have obtained needed written permission statement(s) from the owner(s) of each third-party copyrighted matter to be included in my work, allowing electronic distribution (if such use is not permitted by the fair use doctrine) which will be submitted to UKnowledge as Additional File.

I hereby grant to The University of Kentucky and its agents the irrevocable, non-exclusive, and royalty-free license to archive and make accessible my work in whole or in part in all forms of media, now or hereafter known. I agree that the document mentioned above may be made available immediately for worldwide access unless an embargo applies.

I retain all other ownership rights to the copyright of my work. I also retain the right to use in future works (such as articles or books) all or part of my work. I understand that I am free to register the copyright to my work.

REVIEW, APPROVAL AND ACCEPTANCE

The document mentioned above has been reviewed and accepted by the student's advisor, on behalf of the advisory committee, and by the Director of Graduate Studies (DGS), on behalf of the program; we verify that this is the final, approved version of the student's thesis including all changes required by the advisory committee. The undersigned agree to abide by the statements above.

Nicholas W. Carrara, Student

Dr. Jakub Famulski, Major Professor

Dr. David Westneat, Director of Graduate Studies

ELUCIDATING THE ROLE OF NIDOGEN
IN THE FUSION OF THE CHOROID FISSURE

THESIS

A thesis submitted in partial fulfillment of the
requirements for the degree of Master of Science
in the College of Arts and Sciences
at the University of Kentucky

By

Nicholas W. Carrara

Lexington, Kentucky

Director: Dr. Jakub Famulski, Assistant Professor of Biology

Lexington, Kentucky

2018

Copyright © Nicholas W. Carrara 2018

ABSTRACT OF THESIS

ELUCIDATING THE ROLE OF NIDOGEN IN THE FUSION OF THE CHOROID FISSURE

In the developing embryo, the timely fusion of opposing epithelial sheets into one uniform layer denotes the completion of several developmental events. Failure of this epithelial sheet fusion event (ESF) within the choroid fissure (CF) is associated with the congenital disorder Ocular Coloboma, and is one of the leading causes of pediatric blindness. A requirement for a highly coordinated dismantling of the basement membrane (BM) to allow for fusion to occur is undoubted, however the underlying mechanisms of this process are poorly understood. Due to its BM crosslinking capabilities, I have hypothesized that the regulation of nidogen plays a crucial role in the disassembly of the BM prior to ESF. Whole mount *in situ* hybridization for all four BM components has revealed that expression of nidogen decreases prior to that of other BM components. Additionally, preliminary IHC data has revealed nidogen and collagenIV deposition within the CF. Further, knock-down of nidogen1a and 1b, or the expression of dominant negative nidogen1b resulted in gross morphological, as well as BM organization defects in developing eyes. Together, these data suggest that nidogen plays a role in regulating the integrity of the BM of the eye and may play a role in its disassembly prior to ESF.

KEYWORDS: nidogen, choroid fissure, epithelial fusion, basement membrane, ocular coloboma

Nicholas W. Carrara

July 30, 2018

ELUCIDATING THE ROLE OF NIDOGEN
IN THE FUSION OF THE CHOROID FISSURE

By

Nicholas W. Carrara

Dr. Jakub Famulski
Director of Thesis

Dr. David Westneat
Director of Graduate Studies

July 30, 2018

ACKNOWLEDGEMENTS

I would like to thank my advisor Dr. Famulski for his expertise and mentorship that made this work possible and to whom I am very grateful. I would like to thank my labmates Warlen, Kristyn, and Megan for your support, for all the laughs, and for keeping me sane. I would like to thank my brothers Jake and Joe, my parents, and all of my family for your tremendous confidence in me (even though you may not understand what I have been studying for the past three years). I would like to thank my committee, Dr. Doug Harrison, Dr. Ann Morris, and Dr. Greg Bix for your feedback and for pushing me to conduct the best research I am capable of. I would like to thank my friends who are the greatest in the world. Lastly I would like to thank my fiancé Emmy for your undying support and love, for always believing in me, and for coming with me to Kentucky, (Go Cats!).

TABLE OF CONTENTS

Acknowledgements.....	iii
List of Tables.....	vi
List of Figure.....	vii
Chapter One: Introduction and Background.....	1
Vertebrate Eye Development.....	1
Fusion of the Choroid Fissure.....	5
Coloboma.....	8
Epithelial Sheet Fusion.....	8
Basement Membrane Structure and Function.....	10
Hypothesis.....	13
Using <i>Danio rerio</i> as a model to Study BM Biology.....	13
Chapter Two: Materials and Methods.....	20
Generation of digoxigenin labeled riboprobes.....	20
Whole mount <i>in situ</i> hybridization.....	20
Genotyping and WISH analysis of nidogen2a mutants.....	21
Morpholino Injections.....	22
Morphant phenotype analysis.....	22
Live imaging analysis.....	23
Whole mount immunohistochemistry.....	24
Generation of dominant negative constructs.....	25
Dominant Negative mRNA injection.....	25
Generation of Dominant Negative Nidogen Tol2 Constructs.....	26
Chapter Three: Results.....	29
Expression and Deposition analysis of nidogen and interacting components...29	29
Whole mount <i>in situ</i> hybridization for nidogen.....	29
Whole mount <i>in situ</i> hybridization for collagenIV.....	31
Whole mount <i>in situ</i> hybridization for laminin.....	32
Whole mount <i>in situ</i> hybridization for Perlecan.....	33
Basement membrane component expression comparison within the choroid fissure.....	34
Nidogen and CollagenIV are deposited in the BM of the developing eye including the choroid fissure.....	35
Functional analysis of nidogen via morpholinos and dominant negative Constructs.....	35
Analysis of a nidogen2a mutant reveals no changes in development.....	36
Nidogen morphants display gross morphological phenotypes.....	37
Nidogen morphants display changes in eye size and shape.....	39
Live imaging of nidogen morphant eyes reveals changes in eye development in real time.....	40

Laminin deposition and basement membrane morphology is altered in nidogen morphants.....	40
Eye patterning gene expression is altered in nidogen morphants.....	41
Reducing nidogen function with a dominant negative construct.....	42
Generating a Nidogen1b dominant negative conditional mutant to target ESF...43	
Chapter Four: Discussion.....	64
Laminin zebrafish mutants display similar phenotypes to nidogen morphants.....	64
How nidogen removal can alter basement membrane dynamics prior to ESF.....	65
Regulation of nidogen and subsequent BM remodeling as a result of expression dynamics.....	66
Protein level regulation of nidogen and subsequent BM remodeling.....	67
Nidogen as a potential regulator of the biomechanical strength of basement membranes and epithelial fusion.....	69
Future directions.....	70
Conclusions.....	71
References.....	73
Vita.....	85

LIST OF TABLES

Table 1, A complete list of PCR Primers used in this study.....	28
Table 2, Nidogen amino acid and nucleotide percent identity matrices.....	44
Table 3, A summary of the expression of all major BM components detected in the choroid fissure of the developing eye.....	45

LIST OF FIGURES

Figure 1, Major factors contributing the lens induction and patterning of the early optic vesicle.....	15
Figure 2, Location of the choroid fissure.....	16
Figure 3, Epithelial sheet fusion as it occurs in the developing vertebrate eye.....	17
Figure 4, A structural schematic of nidogen.....	18
Figure 5, The binding capabilities of nidogen in the Basement membrane.....	19
Figure 6, WISH for all four nidogen orthologues from 24-65hpf.....	46
Figure 7, WISH for all 4 nidogen orthologues from 24-65hpf- dissected eyes.....	47
Figure 8, WISH for all collagenIV genes examined at 24hpf.....	48
Figure 9, WISH for collagen4a1 and collagen4a2 from 24-65hpf.....	49
Figure 10, WISH analysis for all laminin genes examined.....	50
Figure 11, WISH for laminina1, laminina4 and lamininc1 from 24-65hpf.....	51
Figure 12, WISH for perlecan from 24-65hpf.....	52
Figure 13, IHC for nidogen in the zebrafish eye at 24 and 48hpf.....	53
Figure 14, IHC for collagenIV in the developing zebrafish eye at 24 and 48hpf.....	54
Figure 15, Nonsense mediated decay detected in nidogen2a mutants.....	55
Figure 16, Nidogen morpholino analysis at 24hpf- gross morphology.....	56
Figure 17, Nidogen morpholino analysis at 24hpf- eye size and eye shape.....	57
Figure 18, Nidogen morpholino analysis at 48hpf.....	58
Figure, 19, Live imaging of nid1a/1b double morphants from 18hpf to 36hpf.....	59
Figure 20, IHC analysis of laminin deposition in nidogen morphant embryos.....	60
Figure 21, Whole mount in situ hybridization in nidogen1a/1b morphants and WT embryos of genes involved in eye patterning.....	61

Figure 22, Dominant Negative Nidogen1b Phenotypes..... 62

Figure 23, WISH for nidogen1b in transgenic dominant negative nidogen1b embryos
after heat shock..... 63

CHAPTER ONE

INTRODUCTION AND BACKGROUND

Introduction

Organogenesis of the vertebrate eye is a highly complex and remarkably conserved developmental event. Perhaps the most important organ for sensory perception, the development, physiology, and neural circuitry of the eye have been extensively studied over the course of the last century. However, owing to the intricacy of the genetic and molecular mechanisms that govern eye development, along with the significant clinical implications of aberrations within these processes, vision research remains an expanding field. My thesis work has focused on aberrations of epithelial sheet fusion (ESF) of the choroid fissure (CF) which when fails is associated with the congenital blinding disorder ocular coloboma, one of the leading causes of pediatric blindness (Hatton, 2007 and Owochei et al. 2000).

Ocular coloboma is sometimes associated with multi-syndromic disorders that are also, in part, due to the failure ESF during normal development. These disorders often display, Coloboma, **H**ear defects, **A**tresia of the choanae, **R**etardation of **G**rowth and development, and **E**ar abnormalities and are referred to as CHARGE syndrome (Guercio, 2007). Although the phenotypic consequences of failed ESF are readily observable in developed tissue, and are clinically detrimental, the molecular mechanisms underpinning ESF remain elusive. To expand the etiological purview of coloboma, and thereby increase our understanding of the molecular mechanisms that govern ESF in other tissues, I have devoted my graduate training to studying the development of the visual system. More specifically, I have endeavored to elucidate the mechanisms responsible for requisite basement membrane (BM) remodeling prior to ESF using the eye as a model.

Vertebrate Eye Development

The vertebrate eye is derived from three major populations of cells, the neuroepithelium, the surface ectoderm, and neural crest, each giving rise to specific

ocular structures of the mature eye (Fuhrmann et al. 2010). The initiation of vertebrate eye development begins with the specification of presumptive eye tissue at the anterior neural plate deemed the eye field. There has been multiple described eye field transcription factors (EFTFs) whose overlapping patterning and self-regulating feedback mechanisms are necessary for the patterning and maintenance of this specified tissue. Work conducted in *Xenopus* suggests the expression of the transcription factor ET, a member of the *Tbx2* subfamily of transcription factors, is responsible for inducing the expression of *Rx* (retinal homeobox gene) ultimately leading to the upregulation of a suite of EFTFs including a master regulator of eye development *Pax6*, as well as *Six3*, *Lhx2*, *tll* and *Optx2* (Zuber et al. 2003).

Studies in zebrafish have shown the expression of the transcription factor *Rx3* in the anterior forebrain biases cells from a telencephalic fate toward eye field identities (Stigloher et al. 2006). Further, *Rx3* has been shown to negatively regulate canonical WNT signaling, a major regulator of anterior-posterior patterning, thereby suppressing posterior fates at the anterior neural plate (Yin et. al 2014). Therefore, it is not surprising that homozygous zebrafish mutants for *Rx3* lack eyes albeit they do develop a lens of reduced size (Loosli et al. 2003).

Following the specification of the eye field, this singular domain of tissue then splits bi-laterally partitioning tissue that will later give rise to two optic vesicles. The critical signaling mechanism responsible for this bilateral split occurs as a result of Sonic Hedgehog (*Shh*) signaling repressing *Pax6* expression in the center of the eye field. Targeted knockout of *Shh* in mice results in cyclopia as a result of the failure of eye field separation (Chiang et al. 1996). Furthermore, using the zebrafish model, it has been shown that *Shh* is the direct target of the homeobox transcription factor *Six3* acting immediately upstream and promoting the expression of *Shh* (Geng et al. 2008). As such, *Shh* and *Six3* are both essential factors in the separation of the eye field ultimately leading to the development of two optic vesicles.

The first observable morphogenetic indication of eye development occurs after the splitting of the eye field as a bi-lateral evagination of optic vesicle from the embryonic ventral forebrain toward the overlying surface ectoderm. This evagination event is concurrent with the expression of *Rax/Rx* which is thought to, in part, mediate

the elongation and polarization of retinal progenitor cells located laterally within the eye field toward the midline (Rembold, 2006). In medaka (*Oryzias latipes*), these elongated and polarized lateral retinal progenitor cells will migrate toward the midline and ultimately reverse course migrating again laterally toward the forming optic vesicle (Rembold, 2006). In *Rx3* knockout zebrafish, these cellular movements are inhibited and the eye fails to evaginate ultimately leading to anophthalmia (Loosli et al. 2003 and Mathers et. al 1997) suggesting *Rx* gene expression and lateral cellular migration are key drivers of the evagination of the optic vesicle. In addition to changes in cellular morphology and migration, evagination of the optic vesicle is marked by the deposition of a laminin rich BM encasing the eye field (Ivanovitch et al. 2013 and K.K Svoboda et al. 1987).

Following evagination, the optic vesicle will continue to move laterally from the midline until it contacts the overlying surface ectoderm (Zheng et al. 2000). It is at this point, the optic vesicle will both invaginate to become the bi-layered optic cup and induce the overlying surface ectoderm to begin to form the lens (as reviewed by Fuhrman 2010 and Graw, 2010). The induction of the lens from the surface ectoderm requires an intricate crosstalk between two types of tissues. The process of lens induction by the optic vesicle is a highly complex and well-studied developmental event and has been condensed for the purposes of this review (Fig.1).

As the optic vesicle contacts and flattens along the surface of the competent presumptive lens ectoderm, it will release inductive signals instructing the creation of the lens. Signaling factors secreted by the optic vesicle include, *Delta2*, *Bmp4* and *Fgf8*. Following their release these signaling factors trigger the expression of both lens specification and differentiation genes such as *Pax6*, *L-maf*, and *FoxE3* (Ogino et al. 2012). Reciprocally, in mice, it has been determined that Fgfs emanating from the surface ectoderm instruct cells of the distal optic vesicle to assume a neuronal fate via the promotion of *Vsx2* (formerly *Chx10*) and subsequent down regulation of MITF (Horsford et al. 2004, Hyer et al. 1998, Nguyen and Arnhieter 2000).

The newly formed bi-layered optic cup can be classified into two distinct populations of progenitor cells separated by the optic lumen. Cells of the proximal layer, under the instruction of MITF, will flatten into squamous epithelium and give rise to the

retinal pigmented epithelium (RPE) (Burmeister et al. 1996). The distal layer, responding to the expression of *Vsx2*, will remain columnar, thicken, and later differentiate into the cell types that populate neural retina (NR) (Li et al. 2000 and Nguyen et al. 2000). As the optic cup is formed, the presumptive RPE layer will decrease in overall size and the presumptive NR will enlarge as a result of migratory rim involution and proliferation of presumptive RPE cells at the ventral margin of the optic cup to populate the NR (Li et al. 2000).

Cells within the distal layer of the optic cup will later differentiate and stratify into the six types of retinal neurons giving rise to the light sensing tissue at the back of the eye. These include, the retinal ganglion cells, amacrine cells, horizontal cells, bipolar cells, and rod and cone photoreceptors. In addition to the six neuronal cell types, the retina also houses Müller glial cells. Retinal progenitor cells will differentiate in a stepwise manner into each retinal cell type generating a mature laminated retina (Schmitt et al. 1999, Cepko et al. 1996, and Prada et al. 1991). The mature neural retina is comprised of three distinct layers of neurons, the outer nuclear layer, the inner nuclear layer, and the ganglion cell layer. The outer nuclear layer houses the light sensing rod and cone photoreceptors. Bipolar cells, within the inner nuclear layer, integrate and propagate signals from the photoreceptor cells, along with amacrine and horizontal cells, to the ganglion cells. Ganglion cell's axonal projections, bundled within the optic nerve (previously the optic stalk) synapse with neurons within the optic tectum and ultimately visual processing occurs (Masland, 2012 and Graw, 2010).

Although the retinal machinery is responsible for detecting and propagating signals provided by light, it is not the only structure of the eye responsible for visual acuity. The morphogenesis of anterior structures of the eye play an integral role in the structure and function of the visual system via focusing light onto the back of the retina. These structures include the cornea, lens, iris, ciliary body, and the iridocorneal angle (Soules and Link, 2005). These structures are thought to arise from a population of highly migratory neural crest cells termed the periocular mesenchyme (POM) (Creuzet et al. 2005 and Gage et al. 2005). These neural crest derivatives express POM specific transcription factors such as, *Foxc1b*, *Foxd3*, *Pitx2*, *Lmx1b* and the neural crest marker *Sox10* and all have been indicated to play roles in the migration to, and development of

the anterior segment (Seo et al. 2017, Dutton et al. 2001, Bohnsack et a. 2012 and McMahon et a. 2009).

The optic stalk, located ventrally in the retina, connecting the optic cup to the forebrain will later house the axons of the retinal ganglion cells to become the optic nerve. Differentiation of the optic stalk from the RPE and NR is accomplished by the mutual antagonizing effects of *Pax2* and *Pax6* which have been determined to demarcate the boundary between tissues of the optic stalk and the optic cup (Schwarz et al. 200). By driving the ectopic expression of *Pax6* using a *Pax2* promoter in the developing mouse embryo, Schwarz and colleagues observed an infringement of optic cup tissue into the optic stalk. In homozygous *Pax6* mutant mice they detected an expanded expression area for *Pax2* and in the reciprocal experiment, they detected the opposite.

The choroid fissure is a naturally occurring transient gap separating the two epithelial lobes of the optic cup spanning the length of the optic stalk (Schmitt and Dowling 1994) (Fig. 2). The fissure allows for the migration of vasculature precursors to enter into the eye through and subsequently generate the transient hyaloid vasculature network (Hartsock et al. 2014 and Saint-Geniez and D'amore, 2004). Ultimately, to complete the generation of the eye's spheroid anatomy and a fully functional optic stalk requires complete closure of the CF via epithelial sheet fusion (ESF).

Fusion of the Choroid Fissure

The cellular mechanisms of ESF of the choroid fissure have begun to be described using the zebrafish model by Andrea James and colleagues (James et al. 2017). Using confocal microscopy and live imaging, James et al. were able to determine several important hallmarks of ESF of the zebrafish choroid fissure. On a morphological level, ESF of the choroid fissure consists of three major steps (Fig. 3). First, the lobes of the eye destined to fuse align in juxtaposition separated by the basement membrane surrounding each epithelial sheet within the interstitial space. Second, the basement membrane is remodeled and displaced to allow direct cell contact of the two epithelia. Finally, cell contact is made and the fusion of two sheets into one continuous cellular layer occurs.

Experimentally, by using a laminin-111 antibody, it was determined that the breakdown of BM precedes tissue fusion and initiates around 34hpf. James reported that the breakdown of BM components occurs in a bidirectional manner beginning centrally in the eye and proceeding both distally (towards the lens) and proximally (toward the forebrain). James reports that the basement membrane becomes mostly undetectable within the choroid fissure at 48hpf.

To examine at what point tissue fusion occurs, James and colleagues utilized both GFP tagged cellular membranes for a live analysis and immunohistochemistry targeting β -catenin as a proxy for adheren junctions. Notably, like BM breakdown, James et al, suggest that tissue fusion progresses in a bidirectional manner beginning in the center of the CF and moving outward however this does not occur until several hours after the BM is removed. Ultimately these findings provide morphological evidence, that basement membrane removal is completed prior to tissue fusion and therefore a necessary step in ESF of the choroid fissure.

Several projects over the last two decades have generated data describing both transcription and signaling factors required for proper closure of the choroid fissure. Of the genes discovered to play a role in ESF of the choroid fissure *Pax2* is perhaps one of the most well studied (Sanyanusin et. al 1995, Torres et al. 1996, and Bower et al. 2012). Not surprisingly, in both the murine and zebrafish model *Pax2* is expressed in the ventral half of the optic cup, the region in which the choroid fissure is located (Nornes et al. 1999 and Krauss et al. 1991). In humans, mice and zebrafish, null mutations in the *Pax2* gene result in coloboma of the eye, as a result of improper choroid fissure closure, as well as defects in the brain, eye, and kidney suggesting *Pax2* function is conserved across vertebrates (Favor et. al 1996). Using the zebrafish model, it was determined that the upstream regulator of *Pax2* is *Shh* which is a known ventralizing signal of neuro-ectodermal tissue (Lupo et a. 2016 and Ekker et al. 1995).

In the zebrafish, retinoic acid (RA) has also been shown to play a role in the patterning of the ventral region of the eye, promoting *Pax2* expression, and instructing the development of the optic stalk (Hyatt et al. 1996). In fact, when Hyatt and colleagues ectopically exposed dorsal regions of the developing zebrafish retina to high levels of RA, they were able to induce the expression of *Pax2* ultimately generating ventral

features such as an in-folding tissue resembling the choroid fissure. Examined together, these data suggest that proper development and fusion of the choroid fissure, at least in part, relies on both the correct dorsal-ventral patterning of the optic cup as well as expression of *Pax2*.

In addition to *Pax2*, the interplay between Shh signaling and both *Vax1* and *Vax2* transcription factors have been indicated to be required for ESF in the choroid fissure (Take-uchi et al. 2003 and Barbieri et al. 2002). Both *Vax1* and *Vax2* gene expression occurs in overlapping domains encompassing both the area of the optic stalk and ventral retinal tissue. Like in *Pax2* mutants, abrogation of *Vax1*, *Vax2* or a combination of both leads to failed ESF of the choroid fissure and coloboma (Take-uchi et al. 2003). Also like *Pax2*, the ventralizing signaling of *Shh* has been shown to upregulate the expression of both *Vax1* and *Vax2* (Take-uchi et al. 2003). Together, these studies suggest both the ventralizing signals of RA and Shh and the transcription factors *Pax2* and *Vax1/2* are, in some way, responsible for the generation, maintenance, and proper development of the optic stalk and ESF of the choroid fissure.

Moreover, in addition to RA and *Shh* signaling, recent studies in both mice and zebrafish indicate the antagonizing effects of *TGFβ2* induced gene expression on *Bmp* (bone morphogenetic protein) signaling in part supports the development and subsequent closure of the choroid fissure (Knickmeyer et al. 2018). *TGFβ2* mutant mice have been shown to display failed choroid fissure fusion and coloboma (Knickmeyer et al. 2018, and Rahaal et al. 2009). Knickmeyer and colleagues determined that in *TGFβ2* knockout mice the expression of two *Bmp* antagonists at the choroid fissure margins, gremlin and follistatin was reduced. In both *Xenopus* and the murine model it has been determined that *Bmp4* is involved in the dorsal patterning of the optic cup (Behesti et al. 2006 and Sasagawa et al. 2004). Therefore, it is likely that *TGFβ2* is involved in maintaining proper dorsal-ventral polarity thereby supporting the proper closure of the choroid fissure via the upregulation of *Bmp* inhibitors in the ventral eye.

Owing to the genetic complexity of ESF of the choroid fissure, there are several other transcription factors and signaling pathways that have been shown play important roles in this event. In addition to those discussed, *CHD7* (Hurd et al. 2007), *Sox11* and *Sox4* (Pillai-Kastoori et al., 2014 and Wen et al. 2015), *YAPI* (Williamson et al. 2014)

and several other, have also been indicated to regulate choroid fissure closure. However broad the scope of genetic and signaling data known to date describing ESF of the choroid fissure, the actual molecular framework and mechanisms required to carry out this process remain elusive.

Coloboma

In the event that ESF of the choroid fissure fails to occur, the resulting clinical phenotype, ocular coloboma arises. As one of the leading causes of pediatric blindness, it has been estimated that 3-11% of blind children worldwide have ocular coloboma (Owochei et al. 2000, Stoll et al. 1992 and MacDonald 1965). According to the NIH, coloboma occurs in 1/10,000 births however as a result of its range of phenotypic severity, likely often goes undiagnosed (nih.gov/condition/coloboma). Although significant advancements have been made in the elucidation of the genetic etiology of coloboma, roughly +80% of patients with the disease have an unidentified causative genetic mutation (Chang et al. 2006, Fitzpatrick and van Heyningen, 2005 and Gregory-Evans et al. 2004). Therefore, it is paramount to increase our understanding of the molecular mechanisms underpinning this ESF event due to the likelihood that deviations within these processes are responsible for the development of coloboma in a potentially large pool of patients.

Epithelial Sheet Fusion

In the developing embryo, the timely fusion of two opposing epithelial sheets into one uniform layer denotes the completion of several developmental events. In addition to the choroid fissure, ESF occurs in the developing palate, heart, neural tube, urethra, eyelids, diaphragm, and uterine ligaments. Although the molecular basis of epithelial fusion events in different organs have some tissue specific mechanisms, many seem to be conserved. These include, the upregulation of adhesion molecules, apoptosis, epithelial

mesenchymal transition, cellular migration, cell signaling, and the use of actin based cellular protrusions (Ray and Niswander, 2012).

A major hallmark of epithelial sheet fusion is the mechanical movement of opposing epithelia into juxtaposition. This migratory behavior is, at least in part, the result of actin based cellular protrusions resembling lamellipodia and filopodia which are the first processes to make contact across tissues during ESF (Pai et al. 2012). Cellular protrusions have been indicated in several epithelial fusion events across species including, dorsal closure in *Drosophila*, and both neural tube and palatal closure in mice (Millard et al. 2008, Taya et al. 1999, Millicovsky and Johnston 1981, and Geelan et al. 1976). It is likely that these protrusions play a role in facilitating the biomechanical force necessary to bridge the anatomical gap separating fusing tissues, and to ‘hold’ tissues in place to allow for subsequent membrane remodeling. It is likely the eye, as other fusing tissues, employs actin based protrusions to complete the fusion process however, it has yet to be determined.

Although the patterns of signaling pathways employed by differing tissue types for ESF are often unique, there are notable overlaps that warrant mentioning. For example, ESF of the palate, neural tube, and heart all have been shown to require ephrin mediated signaling (Stephen et al. 2007, Holmberg et al. 2000, and Orioli et al. 1996,). Both ephrin receptors and ephrin ligands are membrane linked receptor tyrosine kinases and when activated induce intracellular responses as a result of both forward and reverse signaling (Murai et al. 2003). It is also worth noting that ephrins, unlike other receptor tyrosine kinases, do not appear to primarily target the nucleus but have been shown to dramatically alter the cytoskeleton of the cell and regulate cellular shape and movement (Murai et al. 2003). Moreover, rearrangements in cytoskeletal networks have been shown to play significant roles in both epithelial fusion of developing tissues and in the context of wound healing (Woolner et al. 2005 and Jacinto et al. 2001).

In all fusing tissues, adhesion of epithelial sheets following contact is paramount to successfully completing ESF. Studies in mice suggest the transcription factors *Grainyhead-like 2* and *Grainyhead-like 3* (*Grhl2* and *Grhl3*) may regulate ESF via the transcriptional regulation of adhesion molecules (Pyrgaki et al. 2011, Werth et al. 2010 and Rifat et al. 2010). Knockout *Grhl2* mice display multiple ESF defects across tissues,

including the neural tube, the body wall, the palate and even in the choroid fissure (Pyrgaki et al. 2011). Upon further analysis of *Grhl2* mutant mice via microarray it was determined that there were marked changes in E-cadherin expression as well as several genes involved in cell adhesion such as, claudin 4, 6, and 7, epithelial cell adhesion molecule and desmoplakin . Cadherins are a family of cell receptors, who align in a zipper-like fashion and have been shown to play roles in cell adhesion, polarity, and tissue morphology (Shapiro et al. 1995 and Takeichi, 1991). Examined together, it is likely that the timely regulation of adhesion molecules including cadherins, play a key role in facilitating and completing ESF across tissues.

Perhaps one of the most understudied aspects of ESF is the requirement for BM remodeling and removal to allow for cell-cell contact and subsequent adhesion. Although BM removal to allow for tissue fusion is undeniable, the cellular mechanisms regulating this process are still largely unknown. Studies in mice and zebrafish posit BM degradation corresponds with the migration of vasculature precursor neural crest cells through the choroid fissure (Hero et al. 1990 and James et al. 2016). Though this correlation exists, and speculations can be made regarding the mechanisms of these interactions, BM degradation in ESF remains a largely unknown process. Developing a better understanding of how BM remodeling occurs to allow for subsequent fusion will provide valuable insight into the mechanistic etiology of coloboma.

Basement Membrane Structure and Function

BMs are extracellular sheet-like matrices comprised of four major components, laminin, collagenIV, perlecan, and nidogen. These four components self-assemble into supramolecular lattices that serve both structural and physiological purposes for the epithelia that they support (Yurchenco et al. 1990). Emerging roughly 500-700 million years ago along with the evolution of metazoan species, BM components are evolutionarily the oldest extracellular matrix proteins. Relative to their intracellular protein counterparts however, BM proteins are evolutionarily young (Hynes 2012). Genomic comparisons conducted across numerous species have determined remarkable

conservation of all four major basement membrane proteins even in distantly related phyla (Hutter et al. 2000, and Hynes and Zhao, 200). Located at the basal side of every epithelium, basement membranes play important roles in establishing and maintaining tissue borders, cell signaling, and providing biomechanical strength to physiologically active tissues.

Basement membrane architecture is organized along two orders of assembly. First, the molecular structure of each individual component, and second, the supramolecular architecture that results from the interactions of each component. The interactions among individual components are both highly specific and occur with both weak and strong affinities. Basement membranes are not stagnant entities, and it has been determined that both the stoichiometry of their components and biomechanical properties can change over time and during the development of specific tissues (Candiello et al. 2007, Thomas and Dziadek 1994, and Fata et al. 2003). It is important to note, that during the process of ESF the proteins constituting the BM must be targeted and removed efficiently to allow for cell contact to occur. It is therefore crucial to understand how BM components interact with each other and themselves to speculate how remodeling occurs.

Of all the basement membrane components, laminin and collagenIV account for the greatest mass and generate the bulk of the scaffolding network responsible for BM structure. Laminin is a heterotrimeric cross-shaped protein comprised of α , β , and γ chains (~400kDa-800kDa) that plays roles in both BM structure and cell binding via integrins (Tryggvason, 1993). Genetic analyses have suggested that laminin provides the primary structural framework required for the recruitment and organization of other major BM components (Li et al. 2003). The terminal domain of laminin's long arm is responsible for both cell adhesion and self-assembly into polymers while the ends of laminin's short arms (β and γ) are required for the formation of dimers and oligomers.

The second most abundant protein in the BM, collagenIV, is derived from the three polypeptide domains $\alpha 1$, $\alpha 2$ and a globular domain NC1 at the COOH terminus (~550kDa). CollagenIV's NH₂ interacts with three other collagenIV proteins resulting in collagenIV's characteristic chicken wire shaped quaternary assemblage. This uniquely shaped arrangement increases the elasticity of the matrix and ultimately its biomechanical strength. Notably, collagenIV and laminin do not interact independently and therefore

rely on binding to nidogen in order to establish a structural bridge thereby physically linking the two networks.

Perlecan, the most prominent proteoglycan, consists of a 400-500kDa (80nm) core protein attached to three heparan sulfate and/or chondroitin sulfate chains (70kDa-100kDa each) (Paulsson et al. 1987 and Timpl, 1993). It has been indicated as a key regulator of BM signaling. Through its heparan sulfate additions, perlecan has been observed to sequester FGF-2 and mediate binding and delivery to FGF receptors (Smith et al. 2007). In this system, perlecan has been shown to mediate the distribution and bioavailability of cell signaling ligands directly influencing cellular responses as a result of RTK activation. Like both laminin and collagenIV, perlecan has been shown to bind nidogen via the C-terminus of its fifth domain. This interaction is likely involved in the incorporation of perlecan into the BM and thereby maintaining the stability of the BM.

Nidogen is a relatively small BM protein (~150Kd) comprised of three globular domains separated by two spacer regions (Fig. 4). Nidogen's largest β -barrel shaped domain G2 has the ability to bind to both collagenIV and perlecan, while its G3 domain binds to the χ chain of laminin. Early biochemical analyses discovered laminin void of nidogen, as well as a variety of proteolysed laminin fragments, were unable to bind to collagenIV. However, upon its interaction with nidogen, laminin was shown via electron microscopy to bind 8nm away from the C-terminus of the collagenIV triple helix. Furthermore, unlike laminin, dissociated nidogen still maintains its binding affinity for collagenIV (Aumailley et al. 1989). Nidogen is therefore an important crosslinking molecule whose function is to act as a structural bridge between the laminin and collagenIV networks to increase BM stability (Fig. 5).

The importance of nidogen's role in the BM stability has been observed in studies of nidogen null mice. Mice deficient for both nidogen1 and 2 displayed perinatal lethality as a result of BM defects in the heart, lung and kidney (Bader et al. 2005). Further, loss of nidogen has resulted in disrupted basement membrane integrity of the developing mouse apical ectodermal ridge resulting in subsequent defects in limb development (Bose et al. 2006). Additionally, mice deficient for nidogen1 or nidogen2 displayed impaired wound healing suggesting even in adult tissue, impaired BM stability via the deletion of nidogen has an effect on ESF (Baranowsky et al. 2010). Taken together, data generated from these

studies suggest nidogen function is vital to the stability and integrity of both embryonic and adult BMs.

Hypothesis

Nidogen's well characterized crosslinking capabilities, and therefore innate architectural importance, render it a critical link in the structure of the BM; its removal may serve as an efficient and rapid method for BM remodeling prior to ESF in the choroid fissure. Moreover, early work examining the proteolytic vulnerability of BM proteins has discovered nidogen to be the most soluble and most proteolytically susceptible BM component, especially in embryonic tissue (Mayer et al. 1993/1994, Sires et al. 1993). Considering nidogen's key features, I have proposed the following hypothesis: **The removal of nidogen from the BM results in the immediate disassembly of laminin, collagenIV, and perlecan allowing for efficient BM remodeling prior to ESF.** To test this hypothesis, I have employed the zebrafish embryo model system.

Using *Danio rerio* as a model to Study BM Biology

The advantages of using the zebrafish as model for eye development and extracellular matrix biology are abundant. Zebrafish routinely produce large clutches of rapidly developing embryos allowing for large sample sizes. A testament to its rapid development time, the zebrafish embryo has a fully functional eye and can begin tracking movement as early as 72hpf (Easter and Nicola, 1995). Moreover, all development occurs outside the body of the mother within a transparent chorion and embryos are initially unpigmented allowing for one to monitor developmental processes unobstructed. Additionally, the housing of a large stock of zebrafish requires relatively little maintenance and a limited number of reagents which in turn produces a cost effective and space efficient model.

Perhaps most importantly, the developmental processes surrounding ocular development closely mirror that which are found in humans. In fact, the anatomy, histology, circuitry and biochemistry of the eye have been found to be highly conserved among most classes of vertebrates. The morphogenesis of the eye and lens in the developing zebrafish as well as the expression of transcription factors show high levels of conservation with other vertebrates (Fadool and Dowling 2008). Because of this high conservation, zebrafish have become an increasingly important model for studying human diseases including those effecting the eye and visual system (Morris, 2011, Bibliowicz et al. 2011, and Amsterdam and Hopkins 2006).

Finally, the zebrafish model is becoming an increasingly important tool in studying extracellular matrix biology (Feitosa et al. 2011, Wyatt et al. 2009, and Parsons et al. 2002). Owing to the high conservation of BM components across vertebrates coupled with the relative ease for imaging and genetic manipulation, the zebrafish is a uniquely fitted model to study the extracellular matrix.

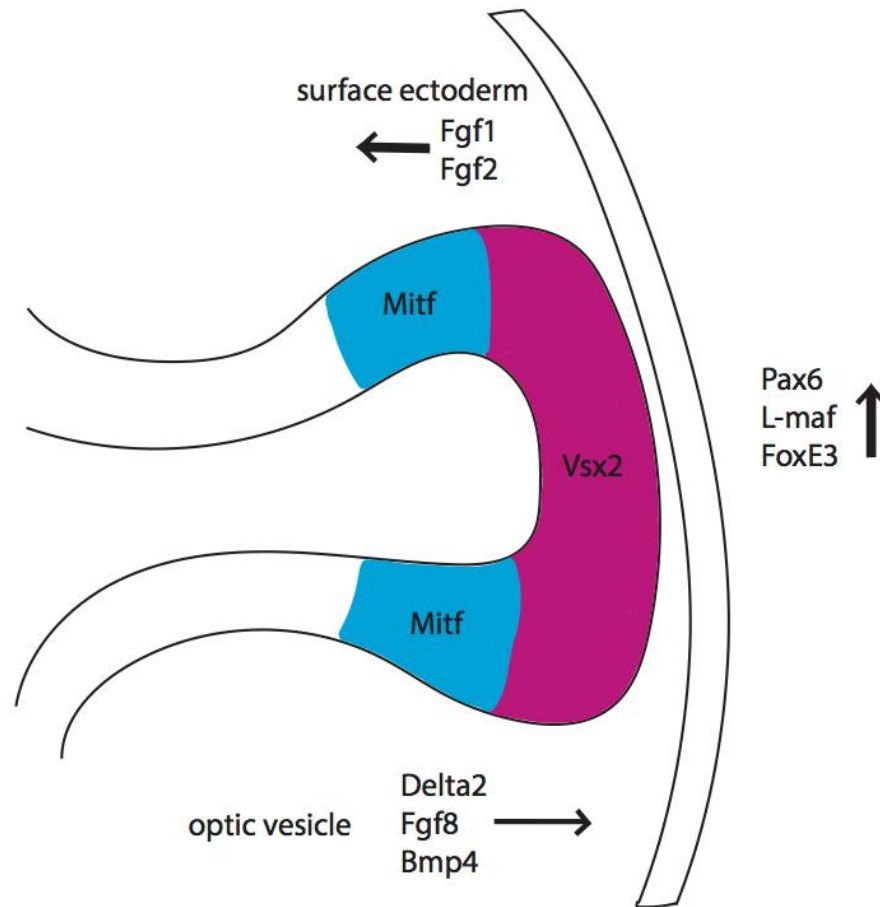


Figure 1. Major factors contributing the lens induction and patterning of the early optic vesicle

The evaginating optic vesicle will induce the overlying surface ectoderm to form a lens by releasing the signaling molecules *Delta2*, *Fgf8*, and *Bmp4*. This will induce the transcription of lens specification genes within the surface ectoderm including *Pax6*, *L-maf* and *FoxE3*.

Reciprocally, the overlying surface ectoderm will release the signaling factors *Fgf1* and *Fgf2* inducing *Vsx2* in the distal optic vesicle which will ultimately lead cells within this region to adopt a neuronal fate. *Mitf*, will be inhibited in the distal optic vesicle and will instruct cells more proximally to become the RPE.

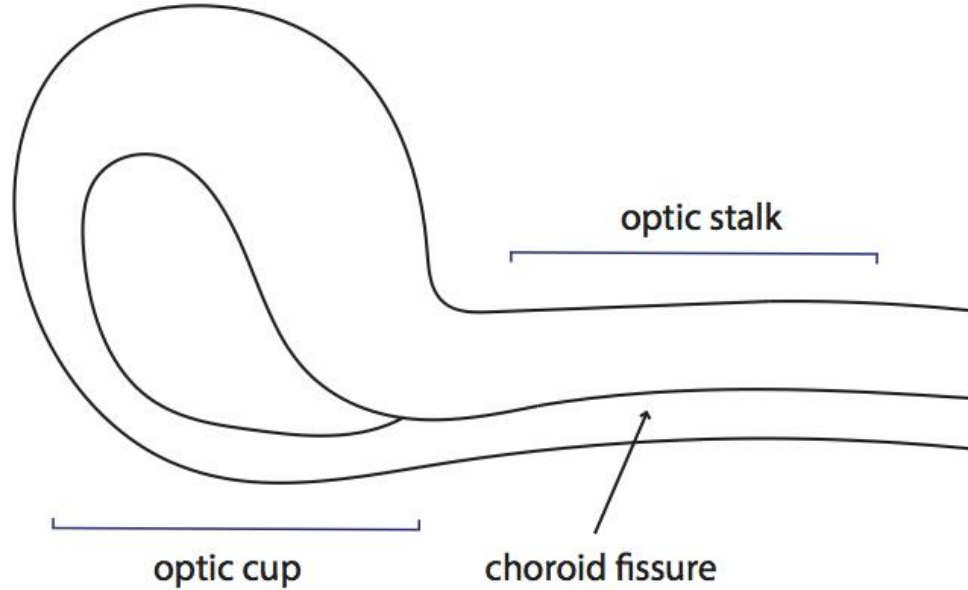


Figure 2. Location of the choroid fissure

The choroid fissure is located ventrally in the developing eye and is located at the optic cup and spans the length of the optic stalk. The choroid fissure will undergo ESF and the optic stalk will constrict to form the optic nerve. The resulting morphology will resemble a continuous spheroid eye connected to the optic nerve.

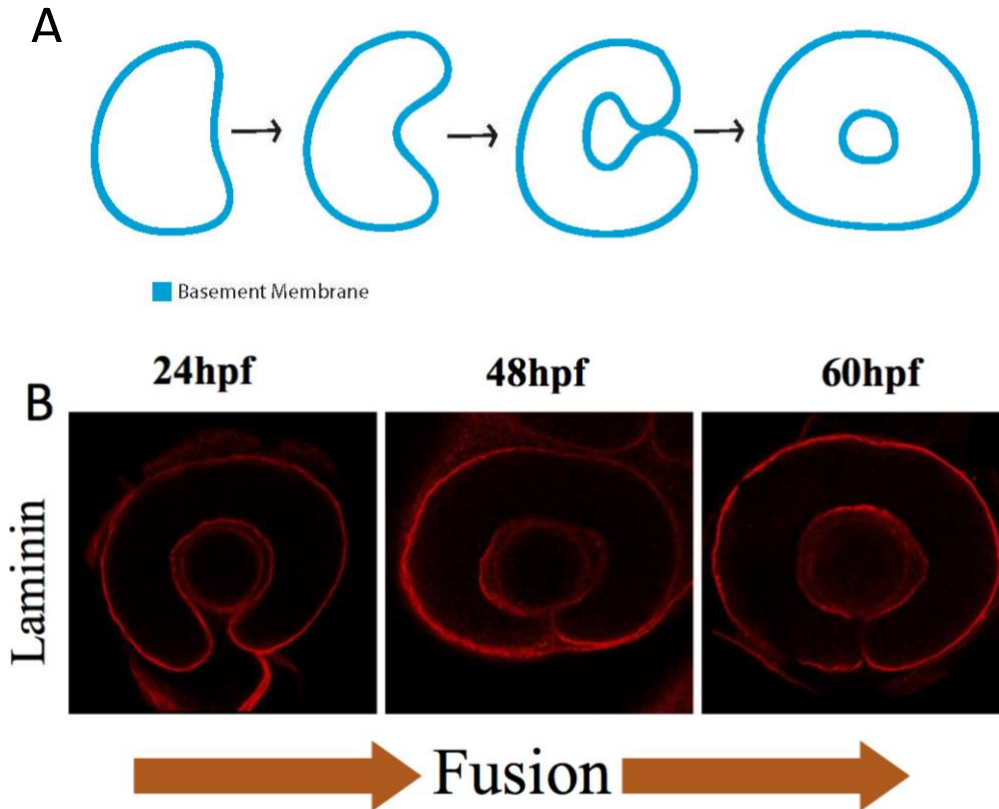


Figure 3. Epithelial sheet fusion as it occurs in the developing vertebrate eye

A) A cross sectional schematic of the developing vertebrate eye. As the eye develops from the flat optic vesicle, it will undergo a series of morphogenetic movements ultimately resulting in a hollow tube-like structure. In order to fuse into one continuous layer of cells, the basement membrane (blue) must be dismantled to allow for cell to cell contact to occur and a fusion of the tissue. **B)** IHC staining of laminin111 during early development of the zebrafish eye undergoing epithelial sheet fusion of the choroid fissure. Laminin (red), a proxy for the basement membrane, is actively removed to allow for cell fusion to occur. This process is completed at approximately 72hpf where laminin even in the most distal region of the eye is undetectable in the choroid fissure.

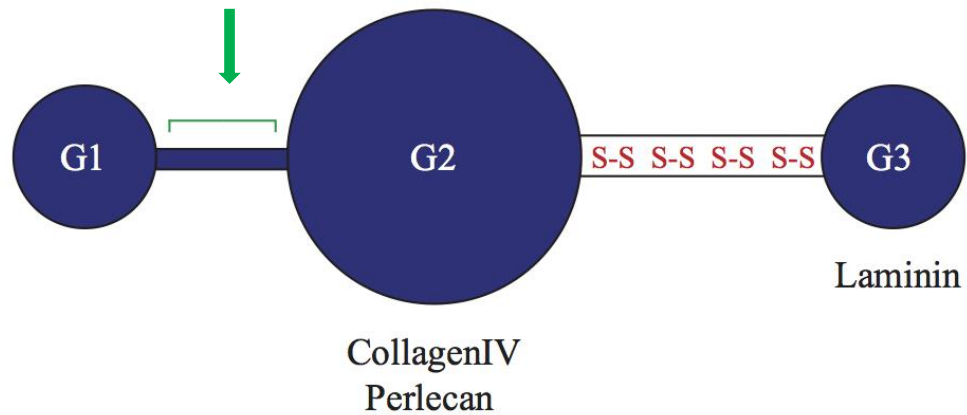


Figure 4. A structural schematic of nidogen

Nidogen protein structure is distinctly dumbbell shaped and is the smallest of the four major basement membrane components (150kD). Nidogens 3 globular domains and 2 spacer regions are important for the function of the protein. Nidogen's globular G2 domain is responsible for binding both Perlecan and CollagenIV network while the G3 domain binds to the laminin network. Sites particularly susceptible to proteolytic cleavage are found within the spacer region between nidogen's G1 and G2 domains (denoted by arrow and green bar). The region most resistant to proteolytic cleavage lies in the spacer region between nidogen's G2 and G3 domain primarily due to disulfide bridges (red S-S).

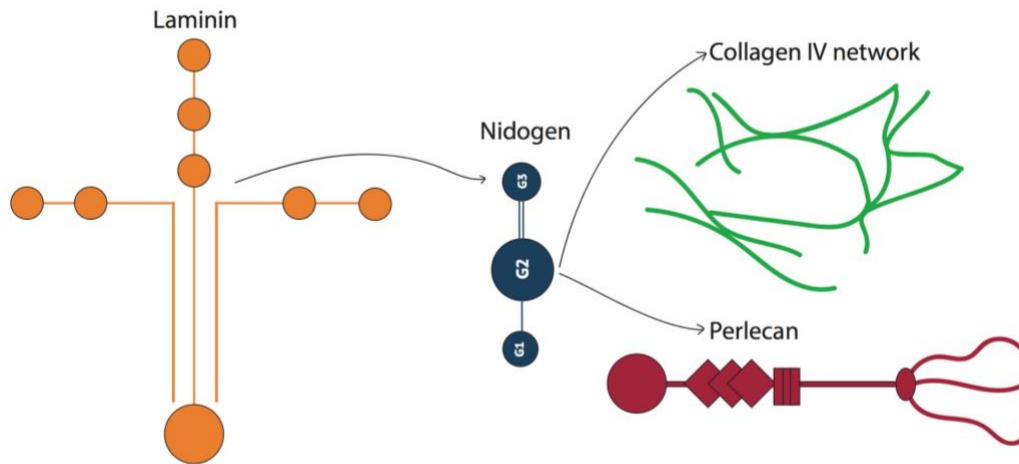


Figure 5. The binding capabilities of nidogen in the Basement membrane.

The basic components of all BMs consist of laminin, perlecan, collagen IV, and nidogen. Nidogen's globular domain G3 binds to the $\gamma 1$ chain of the heterotrimeric protein laminin while its G2 domain binds perlecan and collagen IV. Laminin does not contain a binding site for collagen IV or perlecan. Laminin therefore relies on binding to nidogen in order to establish a structural bridge between itself and other components of the basement membrane.

CHAPTER TWO

MATERIALS and METHODS

Generation of *digoxigenin* labeled riboprobes

To generate riboprobes for whole mount in situ hybridization, riboprobe templates were generated using PCR from pools of 24hpf total cDNA generated via reverse transcription using the Maxima H-minus First Strand cDNA synthesis kit (Thermo) from total RNA extracted using the RNAqueous phenol-free total RNA isolation kit (Ambion) from 24hpf embryos. Primers used are outlined in Table 1 and have T7 RNA binding sites added to the reverse primer for subsequent transcription. *in vitro* transcription was conducted using T7 RNA polymerase along with DIG labelling mix. Probes were purified via exclusion column (Sigma) and were stored at -80°C. WISH probes were diluted 1/200 in 1ml aliquots of hybridization buffer (50% formamide, 20X saline sodium citrate buffer (SSC), 50 mg/ml heparin sulfate, 1M citric acid, 20% Tween-20 and sterile water) for later use.

Whole mount in situ hybridization (WISH)

Embryos were manually dechorionated and fixed with 4% paraformaldehyde (PFA) for a minimum of 2 hours at room temperature or overnight at 4°C. After fixation embryos were washed in phosphate buffer solution with tween (PBS and 0.1% Tween-20) 4 times for 5 minutes. Embryos were then permeabilized with 10mg/ml proteinase K in PBST at room temperature for 6min-30min depending on the age of the embryo. After permeabilization embryos were incubated twice in PBST for 5 minutes and placed in pre-hybridization solution (50% formamide, 20X saline sodium citrate buffer (SSC), 50 mg/ml heparin sulfate, 1M citric acid, 20% Tween-20, tRNA and sterile water) for a minimum of 2 h at 65°C. following pre-hybridization riboprobes were hybridized overnight at 65°C. Embryos were then washed through a series of graded SSC washes at 65°C (66% hyb/33% 2XSSC, 33% hyb/66% 2XSSC, 0.2 SSC/0.1% Tween, 0.1%

SSC/0.1% Tween) and then through a series of graded PBST washes (66%0.2SSC/ 33% PBST, 33%0.2 SSC/66% PBST, PBST) at room temperature. Embryos were then blocked using 2% sheep serum and 2mg/ml bovine serum albumin (BSA) in PBST for a minimum of 1 hour at room temperature. Following the block embryos were incubated with a 1/5000 dilution of anti-*digoxigenin* antibody in blocking solution overnight at 4°C. The following day embryos were washed with PBST 4 times for 10 minutes and then 4 times in coloration buffer (1M tris-HCL pH 9.5, 1M MgCl₂, 5M NaCl, 20% tween-20, and sterile H₂O) for 5 minutes. Embryos were then incubated in coloration buffer with 4-nitro blue tetrazolium (NBT) and 5-bromo-4-chloro-3- indolyl-phosphate, 4-toluidine salt (BCIP) at room temperature or at 37 °C to enhance reaction speed. Coloration was halted by washing in stop solution (PBST pH 5.5) and embryos were imaged using a dissection scope and/or eyes were manually removed, mounted on slides in glycerol and imaged using differential interference contrast (DIC) microscopy at 20x.

Genotyping and WISH analysis of *nidogen2a* mutants

Nidogen2a heterozygous mutants were purchased from ZIRC and were genotyped via an RFLP analysis. To do this, adult zebrafish containing a potential mutation in the *nidogen2a* gene were placed into water treated with Tricaine (3-amino benzoic acidethylester) until they were no longer swimming and were sufficiently anesthetized. Adult fish were placed on a petri dish lid and a scalpel sterilized with ethanol was used to remove the distal tip of the tail. Genomic DNA was isolated by placing fin tissue in PCR tubes with 100ul of NaOH and incubating for 5 minutes at 96°C. After incubation tubes were vortexed for 20 seconds and incubated again for 10 minutes at 96°C. Tubes with dissolved tissue were placed on ice for 2 minutes and 10ul of 1M tris pH 8.0 was added. gDNA was stored at -20 until further use.

The RFLP analysis was conducted by amplifying the region of gDNA with the *nidogen2a* mutation using the forward primer: 5'-TGATCCTATTACTCGACAGATAATAAAG3-' and the reverse: 5'-CGTTTGGCAGGCAGTGGCGGC-3'. The resultant 460bp amplicon was digested with ApeKI (NEB) which would recognize and

digest the mutated allele sequence but not the WT allele. Digested bands were visualized using gel electrophoresis. Confirmed heterozygous fish were in-crossed to generate homozygous mutants. Homozygous mutants were confirmed via RFLP analysis conducted as before and were imaged at 24hpf to observe any phenotypic aberrations. WISH analysis was conducted on *nidogen2a* homozygous mutant fish at both 24 and 48hpf and eyes were dissected off embryos for further expression analysis using the methods previously described.

Morpholino Injections

Translation blocking Morpholinos were obtained from Gene Tools, LLC and used to knock down the expression of *nidogen1a* and *nidogen1b*. The following morpholinos were used in this study: Control MO: 5'-CCTCTTACCTCAGTTACAATTTATA-3', *nidogen1a*: 5'-GTGCCGACCCATATCCAGTCCCAA-3', and *nidogen1b*: 5'-CGGCATCTTCCCCAGGTAGTCAGAC-3'. Morpholino sequences were chosen using ensemble targeting the transcriptional start sites of both *nidogen1a* and *1b*.

Precipitated oligos were suspended in sterile water to a concentration of 20ng/ul. Morpholinos for each gene were injected into fertilized one cell stage WT (AB) and *nid2a*^{-/-} embryos prior to the second cell division. Morpholino concentrations for ABs were 1ng and 2ng of *nid1a* and *1b* independently, and 1ng and 2ng of *nid1a/1b*. Morpholino concentrations injected into *nid2a*^{-/-} embryos were *nid1a/1b* at .5ng, .75ng and 1ng. After injection, all embryos were transferred to fresh embryo media (1.75% NaCl, 0.075% KCl, 0.29% CaCl₂·2H₂O, 0.041% KH₂PO₄, .0142% MgSO₄·7H₂O in 1L of H₂O) and grown in an incubator at 28 °C until fixation.

Morphant phenotype analysis

Morphant embryos were manually dechorionated and fixed in 4% PFA overnight 24 and 48 hours after subsequent injection. At 24hpf morphant embryos were

categorized, imaged using a dissection microscope, separated based on gross phenotypic response, and stored in PBST for laminin immunohistochemistry. Morphants were organized into four categories WT, mild, severe, and lethal. WT embryos were undistinguishable from uninjected or control morphant embryos. Mild embryos had a slight curvature of the tail, a slightly elongated eye (nasal/temporal axis), and mild cloudiness in regions of the brain. Severe embryos had a robust curvature of the tail, a markedly smaller eye, and readily observable cloudiness and indistinguishable brain features. Lethal embryos were categorized as any phenotypic response more robust than severe. Of 48hpf nidogen morphant embryos those displaying a gross morphological phenotype exhibited cloudiness in the areas of the brain, a flattened head and misshapen eye compared to controls. 48hpf fish were categorized into two groups, those displaying a gross phenotypic response and those indistinguishable from WT.

Following image capture, ImageJ software was used to quantify parameters of the morphant embryo eyes at 24hpf and 48hpf. To obtain a measurement of eye size, the area of the eye, measured in pixels (px) was divided by the length of the embryo (px) (from the distal tip of the head to the end of the tail) to normalize for variable embryo size. To obtain a measurement of eye shape, the embryos were positioned laterally, and the length of the nasal/temporal (NT) axis was measured (px) as well as the dorsal/ventral (DV) axis was measured (px) and the ratio of the two (NT/DV) was calculated and recorded. Statistical analysis was conducted using Microsoft Excel Data Package. Student T-tests were conducted between all treatment groups for each parameter measured. The significance cutoff was $P < .005$ and graphical depictions were generated to illustrate results.

Live imaging analysis

Live imaging of nidogen1a/1b morphant embryos was conducted using a Nikon C2+ confocal microscope. 2ng of nidogen1a and 1b morpholino were injected into 1 cell stage of RX3:GFP positive embryos so the tissues of the developing eye were observable over the course of imaging. 18hpf Embryos were imbedded in 1% low gelling agarose in

1-inch glass bottomed Flourodish cell culture dishes (World Precision Instruments) and covered in embryo media, 3-amino benzoic acid ethylester (tricaine) to anaesthetize the embryos and 1-phenyl 2-thiourea (PTU) to inhibit pigmentation. Embryos were imaged over the course of 18 hours from 18hpf to 36hpf during which time the temperature was monitored and on average remained between 28-30 °C to not cause developmental delay. 325 z-stacks at approximately 3µm were taken every five minutes encompassing the entire developing eye throughout the time course. Arevis 4D software was used to analyze the movie.

Whole mount immunohistochemistry (IHC)

For IHC embryos were manually dechorionated and fixed in fresh 4% PFA for 1 to 2 hours at room temperature. Embryos were then washed sequentially in PBST and permeabilized with proteinase K (30ug/mL in PBST) for 5-15 minutes at room temperature. following permeabilization embryos were again washed in PBST and blocked (10% goat serum, 1% BSA, 0.8% Triton X-100, in 1XPBS) for 1-3 days at 4°C. following the block, embryos were incubated in primary antibody (1/25 for nidogen, 1/50 for laminin) in incubation buffer (1% goat serum, 0.8% Triton X-100, 1% BSA, in 1XPBS) for 1-3 days at 4°C. embryos were then thoroughly washed in PBST 5 times for 15 minutes. Then embryos were incubated in secondary antibody conjugated to fluorophores diluted 1/1000 and DAPI in incubation buffer for a minimum of 2 hours in the dark. Secondary Abs were washed off using PBST, 5x for 15min. For confocal imaging (Nikon C2+), embryos were imbedded in 1.2% low gelling agarose in 1-inch glass bottomed Flourodish cell culture dishes. Images of eyes were captured in 3µm stacks spanning from the distal tip of the lens to the back of the eye. Embryos were imaged using a Nikon C2+ confocal microscope.

Generation of dominant negative constructs

Dominant negative mRNA constructs were generated by conducting PCR on pooled cDNA of 24hpf zebrafish embryos using primers found in Table 1. I have designed truncated versions of both nidogen1a and nidogen1b, devoid of their respective G3 domains, which disrupts their ability to link laminin and collagenIV, ultimately destabilizing the structure of the BM. Restriction enzyme sites were added to the cDNA primers used for both constructs for directional cloning (SgsI and XhoI for nidogen2a and EcoRI and XhoI for nidogen1b). After amplification, cDNA templates were ligated into pGEM T-easy plasmids (Promega) and subsequently liberated using restriction enzyme digest. After liberation fragments were then directionally cloned into linearized pCS2+8 plasmids (Addgene) and transformed into chemically competent *E. coli* cells (NEB). Cultures were grown overnight and mini-prepped to isolate plasmid. Plasmids were confirmed using both restriction fragment length polymorphism assays (RFLP) and sequencing (eurofins genomics).

mRNA was generated from confirmed plasmids first by linearization with NotI and then using the Invitrogen mMessage mMachine transcription kit (Sp6). The concentration and purity of mRNA was determined by measuring the optical density and aliquots were stored at -80 °C until injection.

Dominant Negative mRNA injection

Dominant negative mRNA was diluted in RNase free H₂O to the following concentrations: 200pg, 300pg, and 350pg. Aliquots of mRNA were stored on ice throughout the duration of the procedure to inhibit degradation. Dominant negative mRNA was injected into zebrafish embryos using RNase free glass capillary needles at the 1-cell stage with the above stated concentrations. Following injection embryos were transferred directly to embryo media and placed in a 28 °C incubator to develop.

Generation of Dominant Negative Nidogen Tol2 Constructs

Nidogen1b dominant negative heatshock transgenic zebrafish were generated using the Tol2 kit v1.2 (Kwan et al. 2016) and Invitrogen's Multisite Gateway© Three Fragment Vector Construction Kit. PCR was conducted utilizing a previously constructed pGEM-T easy vector (Promega) containing nidogen1b sequence using *attb* flanked nidogen1b dominant negative primers. Once the PCR product was amplified it was combined with pD221 donor plasmid, BP clonase enzyme, BP reaction buffer and TE pH 8.0 for 1 hour at room temperature for recombination. Ligated nidogen1b dominant negative entry clones were transformed into chemically competent *E. coli* (NEB) cells and plated on kanamycin plates and grown overnight at 37 °C. The next day colonies were picked and grown overnight in 2ml of Luria broth (LB) media + kanamycin. Plasmids were isolated via mini-preps (E.N.Z.A plasmid mini kit, Omega) and confirmed via RFLP using *Cla*I restriction enzyme.

To generate an expression construct, the dominant negative nidogen1b donor plasmid was combined with the 5' entry clone p5E-hsp70 (heatshock promoter) and 3' entry clone p3E-polyA (poly A signal) along with the pDestTol2Cred destination vector and LR clonase to generate the expression vector via recombination as follows [heatshock promoter][dominant negative nidogen1b][polyA]. In addition to the fragments above, the destination vector was also equipped with a *cmlc* promoter driving the expression of mCherry. This allowed for the easy identification of transgenic embryos via the observation of a red fluorescent heart. Expression vectors were transformed into chemically competent *E. coli* cells (NEB) and plated on kanamycin plates and grown overnight at 37 °C. Plasmid transformation was confirmed via colony PCR and colonies containing the correct expression construct were grown overnight in 2ml of LB media overnight and mini-prepped the following day for isolation.

To test the construct both AB and *Attb* embryos were co-injected with dominant negative nidogen1b destination vector and Tol2 enzyme prior to the one cell stage. After injection, embryos were raised to 24hpf and embryos with red hearts were subsequently heatshocked for 30min at 38 °C to induce expression of dominant negative nidogen1b. To test whether dominant negative nidogen1b gene expression was induced via heatshock,

WISH was performed for nidogen1b at 24hpf on 25 embryos that displayed red hearts. After mosaic expression was observed, the remaining embryos displaying red hearts were further grown and will be subsequently outcrossed to AB embryos and genotyped to establish a transgenic line.

Table 1. A complete list of PCR Primers used in this study.

WISH Probe Primers		
Probe	Forward (5'-3')	Reverse (5'-3')
nidogen 1a	ATGGGTCGGCACGGGCACAGAC	TAATACGACTCACTCACTATAGGGTCGACCTGTTGTGGG
nidogen 1b	ATGCCGGCTAAGTTTGGCATG	TAATACGACTCACTCACTATAGGGCCATTGCCATAATAACCAGG
nidogen 2a	ATGCTCACGAGCTGCATGTGTAC	TAATACGACTCACTCACTATAGGGCAGAACTCTGTTGTGTGGG
nidogen 2b	GCTGTACTTTTAACAAATGTTTCG	TAATACGACTCACTCACTATAGGGGTAGTCTGTGCAGTATCCATC
laminin a1	ATGATGGAGATGAGGATGAAG	TAATACGACTCACTCACTATAGGGCCATGGCTCCTGATCCTATC
laminin a4	GCGTCCTGTTAACCTGTCGTCC	TAATACGACTCACTCACTATAGGGTCAAGCAGAAGGACAGGCGCC
laminin c1	GAGCGATGGATGGATGAATGTATAG	TAATACGACTCACTCACTATAGGGCAGTTACAAGGCAGACACTC
laminin c2	CTCACGAAGGAGATTGCTGGT	TAATACGACTCACTCACTATAGGGTTATGGCCTTTCATAGGTGG
laminin c3	ATGACCTCTTTCACAGACG	TAATACGACTCACTCACTATAGGGTCAGTGGCCTTTTCTGGGCA
laminin b1b	CAAGACTCCTTAAATAAAGCC	TAATACGACTCACTCACTATAGGGAGCGCGCAGGTGCTGTAGATGTTG
laminin b2	CAACTGCTTCTGCTATGGC	TAATACGACTCACTCACTATAGGGTCTAATCACTACAACACGC
laminin b4	GACTGTCGGGGAGTTTACCC	TAATACGACTCACTCACTATAGGGAGGGGAGCACAGATTGTATCTC
collagen4a3	GGACAAAAGGACAGTGTGGTC	TAATACGACTCACTCACTATAGGGCAAGGTCACCTTGAAGGCTGTTG
collagen4a4	CTGGGTCCCAGTGGTGCAAAG	TAATACGACTCACTCACTATAGGGCATGGTTGGGGTCATTCATC
collagen4a5	GGTTTTCCAGGATCTAAAGGAG	TAATACGACTCACTCACTATAGGGCGTCTCTTCATACACCAC
collagen4a6	CGTCCAGGAATAATAGGACC	TAATACGACTCACTCACTATAGGGCTACAAGATCTTCATGCAGAC
collagen4a1	GGTTCTAAGGGTGAAGGAGGTG	TAATACGACTCACTCACTATAGGGCCCTCTTCATGCACCTTGAC
collagen4a2	CCTAAAGGAGATACCGGACCC	TAATACGACTCACTCACTATAGGGCTACAGGTTCTTCATGCACAC
perlecan	CTTAATATCCACACCAATG	TAATACGACTCACTCACTATAGGGTTATGTAAAGCAGCAGCCGTCTAC
foxg1a	ACAGGAGCAAAGTCGGAG	TAATACGACTCACTCACTATAGGTAGTCAGAAAAGTCCACTGG
foxd1	ATGACTCTGAGCTCCGAGATG	TAATACGACTCACTCACTATAGGGAAGTCCGTGAGGCACAAT
vax2	ATGTTTGATCAAGCCACGAGTATG	TAATACGACTCACTCACTATAGGGTTAGGACACCGTCTTCTTCCC
aldh1a2	ATGACCTCCAGTGAAGTTGAAC	TAATACGACTCACTCACTATAGGGTTAAGACGTCTTGCTGACATC
Dominant Negative Contrsuct Primers		
nidogen1b	GAATTCATGCCGGCTAAGTTTGGCATG	CTCGAGTCAGGCTTTCTGAACACTCGTCC
nidogen2a	GGCGCGCCATGCTCACGAGCTGCATGT	CTCGAGTCAACACGGCTGCTCACCACACT

CHAPTER THREE

RESULTS

Expression and Deposition analysis of nidogen and interacting components

To elucidate the expression dynamics of nidogen and its interacting BM components prior to and during ESF within the choroid fissure, we employed whole mount *in situ* hybridization (WISH). By examining a multitude of zebrafish BM component orthologues at several time points we were not only able to determine which specific zebrafish BM orthologues are expressed in the CF, but how their expression is regulated throughout ESF. Although regulation of nidogen as a means of dismantling the BM to allow for ESF is likely primarily controlled on a protein level, it is possible that duration of each components' expression plays a role in BM structural dynamics. For example, if the expression of *nidogen* within the choroid fissure ceases prior to the expression of laminin, collagenIV, and perlecan this could lead to a stoichiometric imbalance of nidogen within the BM which may ultimately lead to impeded component integration and subsequently decrease BM integrity. To determine whether this is a viable model, we generated a complete chronological expression profile for all BM components prior to and during ESF.

Whole mount in situ hybridization for nidogen

Zebrafish possess four orthologues of the nidogen gene, *nidogen1a*, *nidogen1b*, *nidogen2a* and *nidogen2b* (Table 2). To generate an expression profile for all 4 nidogen orthologues whole mount *in situ* hybridization was analyzed in whole embryos and dissected eyes from 24-65hpf (Fig. 6, and Fig. 7). At 24hpf, the expression of *nidogen1a* (Fig. 6, a1) is most prominent in the developing somites and can also be observed surrounding the developing eye and lens including the choroid fissure. Dorsally, *nidogen1a* expression was observed in the olfactory placode and outlining the midbrain regions (Fig.6, a2). In contrast to *nidogen1a* at 24hpf, *nidogen1b* expression is most prominent in the tissue marking the mid-hindbrain region and at the distal epithelium

surrounding the tail (Fig. 6, b1). Additionally, like *nidogen1a* at 24hpf, *nidogen1b* expression can be observed surrounding the tissue of the developing eye and lens including the choroid fissure. *Nidogen2a* expression at 24hpf is most prominently observed in the anterior region of the embryo outlining the boundaries of the forebrain and hindbrain and at the tip of the developing tail (Fig. 6, c1). Dorsally, at 24hpf *nidogen2a* expression is prominent in the developing olfactory lobes, and like *nidogen1a* and *1b* can be observed in tissues surrounding the eye, lens, and choroid fissure (Fig. 6, c2). *Nidogen2b* expression at 24hpf was observed in the tissues surrounding the developing hind-brain regions (Fig. 6, d1). Dorsally, *nidogen2b* expression is located directly in the tissue at the midline spanning the fore and midbrain and in throughout the hindbrain ventricle (Fig. 6, d2). Interestingly, *nidogen2b* was not expressed in the choroid fissure.

At 36hpf, the spatial expression of *nidogen1a*, *1b*, and *2a* remains relatively unchanged from 24hpf. Notably, the expression of all three of these orthologues is easily observed within the developing choroid fissure (Fig. 6, a3, b3, and c3, and Fig. 7, a3, b3, and e3). Additionally, at 36hpf, the expression of *nidogen1a* and *2a* was observed in the developing gill arches and fin buds (Fig. 6 a4 and c4). At 36hpf, the expression of *nidogen2b* was no longer detectable (Fig. 6, d3 and d4) however, its expression becomes detectable later at 48hpf in the developing otic vesicle (Fig. 6, d5).

At 48hpf the expression of *nidogen1a* is no longer detectable in the head of the embryo (Fig. 6, a5 and a6). The expression of *nidogen1b* persists outlining the mid-hindbrain boundary and developing brain as well as within the choroid fissure (Fig. 6, b5 and b6). *Nidogen2a* expression at 48hpf is observed strongly in the developing fin buds as well as in the developing gill arches (Fig. 6, c5) and faintly within the developing choroid fissure (Fig. 6, c5).

At 56hpf *nidogen1b* is the only detectable orthologue expressed within the choroid fissure (Fig. 6, b7 and Fig. 7, b5). At 56hpf *nidogen1b* was also detected in the areas outlining the brain at the mid-hind brain boundary (Fig. 6, b8). The expression of *nidogen1a* and *2a* were most prominently observed in the developing fin buds (Fig. 6, a8 and c7). At 65hpf no *nidogen* orthologues were observed to be expressed in the choroid

fissure (Fig. 6 a9-c9 and Fig. 7 a6-d6). However, at 65hpf, *nidogen1a*, *1b*, and *2a* expression was detected at the developing fins (Fig. 6 a10-c10).

To generate a clearer view of *nidogen* expression as it pertains to the developing retina, embryonic eyes from WISH treated embryos, were dissected, mounted onto slides and imaged using DIC microscopy (Fig. 7). The expression of *nidogen1a*, *1b* and *2a* were all observed within the developing choroid fissure while *nidogen2b* expression was not detectable in the eye. The expression of *nidogen1a* within the choroid fissure was last detectable at 36hpf (Fig. 7, a3) and was not detected in eye tissue at later time points (Fig. 7, a4-a6). *Nidogen1b* was expressed the longest within the choroid fissure up to 56hpf (Fig. 7, b5). Expression of *nidogen2a* was last detected within the choroid fissure at 48hpf in tissues near the lens (Fig. 7, c4). Although expressed within other developing tissues, the expression of *nidogen1b* was not detected in tissues of the eye (Fig. 7, d1-d6).

Together, these data suggest that each *nidogen* orthologue is expressed in both different and overlapping tissues, but that *nidogen1a*, *1b*, and *2a* are expressed within the choroid fissure. Likely, it is an interplay between *nidogen1a*, *1b*, and *2a* that together integrate into the BM of the CF and subsequently provide the necessary crosslinking of the laminin and collagenIV networks. Additionally, the expression of *nidogen1a* and *2a* cease to be expressed and subsequently deposited into the BM of the CF by 48hpf and 56hpf respectively and *nidogen1b* by 65hpf. To compare the spatial and temporal characteristics of *nidogen* expression to that of their interacting components, we next completed an expression analysis for *collagenIV*, *laminin*, and *perlecan*.

Whole mount in situ hybridization for collagenIV

To elucidate which specific *collagenIV* orthologues are integrated into the BM of the CF, expression profiles were examined for 6 collagenIV zebrafish orthologues: *collagen4a1*, *collagen4a2*, *collagen4a3*, *collagen4a4*, *collagen4a5* and *collagen4a6* at 24hpf (Fig. 8). From this data it was determined that *collagen4a1* and *collagen4a2* were expressed within the choroid fissure (Fig. 8, d1 and d2) and these two genes were further examined (Fig 9).

From 24-65hpf, the expression of both *collagen4a1* and *a2* was observed in the head of the embryo, the tissue surrounding the developing eye and at the anterior and posterior boundaries of the midbrain (Fig. 8 a1-a5 and d1-d5). Expression of both *collagens* was also observed in the developing gill arches from 24-56hpf (Fig. 8 a1-a5 and d1-d5). Additionally, at later time points (56hpf and 65hpf) *collagen4a1* and *a2* expression was detected in the developing fin buds (b4-b5, and e4-e5).

Eyes dissected from collagenIV WISH embryos showed the expression of both orthologues within the choroid fissure from 24hpf to 65hpf (c1-c5 and f1-f5). Contrary to *nidogen* expression which becomes undetectable at 56hpf for *nidogen1b*, the expression of both *collagen4a1* and *a2* persists throughout ESF of the choroid fissure from 24-65hpf. This suggests that at 65hpf, as more collagenIV is deposited into the BM, no additional nidogen is added. This may in turn, reduce the ability of collagenIV to subsequently bind the laminin network thereby decreasing BM stability allowing for ESF.

Whole mount in situ hybridization for laminin

Expression profiles were examined for *laminin a1, a4, b1b, b2, b4, c1, c2, and c3* (Fig. 10). From these data, it was determined *laminin a1, a4, and c1* were expressed within the choroid fissure (Fig. 10, top row, bottom row) and were further examined at later time points (Fig. 11). At 24hpf *laminin a1* expression was observed in anterior regions of the developing embryo outlining the midbrain and the diencephalon (Fig. 11, a1 and a5). Additionally, expression of *laminin a1* was observed in the anterior of the developing embryo outlining the mid-hindbrain boundary, mesencephalon, and diencephalon from 48-65hpf (Fig. 11, a2-a4 and a6-a8). *Laminin a1* expression was also visible in the otic vesicle from 48-65hpf (Fig. 11a2-a4) and in the developing fin buds (Fig. 11, a5-a7). In the developing eye, *laminin a1* expression was observable in the developing choroid fissure from 24-56hpf however it was no longer detectable at 65hpf (Fig. 11, a9-a12).

Laminin a4 24hpf is expressed primarily in the ventral tissues surrounding the yolk, at the mid-hindbrain boundary, and surrounding the eye and choroid fissure (Fig.

11, b1, b5 and b7). Expression of *laminin a4* was also observed in the gill arches and limb buds from 24-56hpf (Fig. 11 b1-b7). Expression of *laminin a4* was no longer detectable within the choroid fissure at 56hpf (Fig. 11, b11). Notably, the expression of *laminin a4* in all anterior regions of the developing embryo ceases by 65hpf and no detectable expression was observed (Fig. 11, b4, b8, and b12).

The expression of *laminin c1* was observably similar to that of *laminin a1* and was detected outlining areas of the mid-hindbrain boundary, the mesencephalon, the gill arches, the otic vesicle and developing fin buds from 24-65hpf (Fig. 11, c1-c8). Expression of *laminin c1*, like that of the other *laminin* orthologues, was no longer detectable within the choroid fissure at 65hpf (Fig. 11, c12).

In summary, the expression of all three laminin genes within the CF (*laminin a1*, *a4*, and *c1*) are detectable at 56hpf but not at 65hpf. In contrast, only one *nidogen* orthologue, *nidogen1b*, is still detectable at 56hpf. Together, these data suggest that while three laminin genes continue to be expressed and likely deposited into the BM of the CF, these newly introduced laminin molecules may not be as efficiently incorporated into the matrix as a result of reduced *nidogen* expression.

Whole mount in situ hybridization for Perlecan

WISH for the one zebrafish orthologue of *perlecan* revealed expression in the anterior regions of the developing embryo including the eye from 24-65hpf (Fig. 12). At 24hpf *perlecan* expression was observed surrounding regions of the brain including the mesencephalon, the midbrain and the hindbrain and was also observed in both the choroid fissure and the lens (Fig. 11, a, e, and i). From 48-65hpf *perlecan* expression continued to be expressed in areas outlining the mesencephalon and at the mid-hindbrain boundary (Fig. 11, j-l). Additionally, expression was also observed in the developing fin buds (Fig. 11, k-l). In the eye, expression of *perlecan* was observed both within the choroid fissure and the lens from 24-65hpf (Fig. 11 a-d). Parallel to *collagen4a1* and *a2* the expression of *perlecan* persists throughout the processes of ESF. Like both laminin and collagenIV, perlecan interacts with nidogen via the C-terminus of its V domain likely

playing a role in its integration into the BM (Brown et al. 1997). It is therefore possible, that in conditions with reduced nidogen expression, as have been observed in late ESF, the ability of newly expressed perlecan to interact and integrate within the BM of the choroid fissure is likely impeded.

Basement membrane component expression comparison within the choroid fissure

A comparative table illustrating the expression profile of all BM genes expressed in the choroid fissure was generated using WISH results (Table 3). Of all the BM genes discovered to be expressed within the choroid fissure, the *nidogens* lose detectability prior to the *collagens*, *laminins*, and *perlecan*. Specifically, the expression of *nidogen1a* ceases the earliest of all BM components (at 48hpf), followed by the other two *nidogen* genes expressed in the eye *nidogen1b* and *2a* (56hpf and 48hpf respectively) (the expression of *nidogen2b* was not detected in the eye). While the expression of only one of the *nidogen* orthologues could be detected at 56hpf (*nidogen1b*), the expression of *laminina1*, *a4*, and *c1*, *collagen4a1* and *a2*, and *perlecan* is still detectable within the fissure at this time. Further, the expression *collagen4a1*, *a2* and *perlecan* can be detected in the choroid fissure as late at 65 hpf at which point the fusion of the majority of the choroid fissure has completed (James et al. 2016).

The temporal characteristics of the expression of all BM genes examined, specifically, the discovery that nidogen gene expression ceases prior to that of its interacting components within the CF may result in biomechanical consequences of the BM. For example, expression of BM components within the choroid fissure during a time where BM disassembly is eminent may be perceived as counterproductive however, if these components fail to integrate into the BM as a result of a nidogen deficit, efficient breakdown of the BM is still wholly possible.

Nidogen and CollagenIV are deposited in the BM of the developing eye including the choroid fissure

As suggested earlier, the breakdown of the BM to allow for ESF is likely an interplay between both expression dynamics, and protein stability regulation via remodeling enzymes. To understand how different BM components behave on a protein level during BM breakdown, we have begun to examine the deposition of both collagenIV and nidogen within the CF. It is the ultimate goal of these experiments to, akin to the previous expression analysis, create a complete spatiotemporal protein stability profile of all BM components and generate a chronology of their breakdown. The following work is currently in processes and is yet to be completed.

IHC was conducted using α -rabbit antibodies against collagenIV and nidogen in the developing eye at 24 and 48hpf (Fig. 13 and Fig. 14). Nidogen deposition was detected using a mixture of α -rabbit nidogen1 and 2 antibodies at both 24 and 48hpf in the BM surrounding the lobes of the eyes as shown in figure 13. Nidogen deposition was also observed in the BMs outlining the somites in the developing tail at 24hpf (Fig. 13, right column). Detection of nidogen deposition at later time points failed possibly as a result of failed antigen retrieval.

Moreover, IHC for collagen4 was conducted using α -rabbit collagenIV antibodies (Fig. 14). CollagenIV deposition was detected both in the BM surrounding the lobes of the developing eye and within the BM surrounding the lens at both 24 and 48hpf. Like nidogen, the detection of collagenIV at later time points failed and needs to be worked repeated. Although much remains to be discovered about the dynamic breakdown of different BM components prior to ESF, I hypothesize that the initial targeting of nidogen for degradation results in the most efficient and rapid mechanism for BM disassembly.

Functional analysis of nidogen via morpholinos and dominant negative constructs

To generate a clearer understanding of morphological consequences as a result of weakened BMs by reducing nidogen function, I have taken three approaches. I have

examined a *nidogen2a* mutant, I have used translation blocking *nidogen* morpholinos, and I have generated and employed dominant negative *nidogen1b* constructs. Previous work examining *nidogen* loss of function in the mouse model has shown that lack of *nidogen1* and *2* results in BM defects in multiple tissues including, the heart and the lungs ultimately resulting in perinatal lethality (Bader et al. 2005). Additionally, loss of *nidogen* function in the mouse model has been shown to result in impaired limb development as a result of irregular BM composition at the apical ectodermal ridge (AER) (Bose et al. 2006). Therefore, we thought it likely, that deterring *nidogen* function in the zebrafish model would impede BM development and provide similar results.

Analysis of a *nidogen2a* mutant reveals no changes in development

A *nidogen2a* mutant was obtained from the Zebrafish International Resource Center (ZIRC) in which the mutant allele possessed a C>T mutation resulting in a premature stop codon. The resultant mutant protein is severely truncated (mutant: 473 amino acids, WT: 1351 amino acids) and void of both its G2 and G3 domains and is therefore nonfunctional. The morphology of homozygous *nidogen2a* mutants showed no phenotypic aberrations compared to WT embryos at 24 or 48hpf (Fig. 21 a, e, d, and h). A WISH analysis for *nidogen2a* in *nidogen2a* mutants showed a marked decrease in *nidogen2a* transcript abundance which is likely a result of nonsense mediated decay of the faulty transcript at both 24 and 48hpf in the eye. Previously recorded results examining knockout of murine *nidogen1* and *nidogen2* have shown genetic compensation occurs between the *nidogens* (Bader et al. 2005). Additionally, given that zebrafish possess not two, but four *nidogen* genes which likely have overlapping function and ability to compensate for one another makes it not surprising that no phenotype was observed in *nidogen2a* mutant embryos.

Nidogen morphants display gross morphological phenotypes

To determine if knocking down the function of nidogen in the developing embryo had an effect on overall development we took advantage of morpholinos. Translation blocking morpholinos were used to knock down the expression of *nidogen1a* and *nidogen1b* in both WT and *nidogen2a*^{-/-} embryos. Nidogen1a and nidogen1b morpholinos were injected into AB embryos independently at 1ng and 2ng or in combination. *Nidogen2a*^{-/-} embryos were injected with a combination of nidogen1a and 1b morpholinos but at reduced concentrations (.5ng, .75ng, 1ng). Nidogen morphant embryos displayed gross morphological aberrations and were categorized based on robustness of phenotype outlined in Figure 15 A. Nidogen morphants displayed an array of phenotypes that were organized into four increasingly robust categories: WT, mild, severe, and lethal. WT classified embryos were undistinguishable from uninjected or control morphant embryos. Mild classified embryos had a slight curvature of the tail, a slightly elongated eye (nasal/temporal axis), and mild cloudiness in regions of the brain. Severe classified embryos had a robust curvature of the tail, a markedly smaller eye, and readily observable cloudiness and indistinguishable brain features. Lethal embryos were categorized as any phenotypic response to morpholino more robust than severe.

Injecting a control MO into WT embryos at a concentration of 2ng resulted in 97% of embryos that were indistinguishable from WT with only 3% displaying mild phenotypes at 24hpf (Fig. 15, B.). Knockdown of *nidogen1a* and 1b independently in WT embryos resulted in a dose dependent phenotypic response at 24hpf. Using 1ng of morpholino to knock down both *nidogen* genes independently resulted in gross morphological phenotypes in 37% of *nidogen1a* morphants (34% moderate and 3% severe) and 49% of *nidogen1b* morphants (39% moderate and 10% severe) at 24hpf. When the concentration for each independent injection was increased to 2ng, the percent of embryos that displayed morphological phenotypes rose to 57% in *nidogen1a* morphants (31% moderate, 52% severe, and 2% lethal) and 83% in *nidogen1b* morphants (54% moderate, 17% severe, and 12% lethal) in a dose dependent manner.

To determine whether *nidogen1a* and *nidogen1b* have synergistic function, we then targeted both transcripts simultaneously for knockdown. Knockdown of

nidogen1a/1b in combination resulted in 95% of embryos displaying morphological phenotypes (5% WT, 40% mild, 49% severe, and 6% lethal) even at the lower concentration of 1ng at 24hpf. When the concentration of nidogen1a/1b morpholinos was increased to 2ng each this resulted in 85% of embryos displaying a phenotypic response (15% WT, 19% mild, 53% severe, and 13% lethal phenotypes), but a greater percent of embryos displayed lethal phenotypes (13% in 2ng treatment to 6% in 1ng treatment). This suggests that nidogen1a and nidogen1b have synergistic functionality and when knocked down in unison result in a very high percentage of embryos which display robust phenotypes.

To observe whether these phenotypes persisted later in development morphant embryos were also examined at 48hpf and categorized into those displaying morphological phenotypes and those indistinguishable from WT (Fig. 17, A-B). Morphants displaying phenotypes displayed flattened head, misshapen eyes, heart edema, and cloudiness of the head. Nidogen1a 48hpf morphants displayed a dose response from 1ng to 2ng with 33% and 67% showing gross morphological phenotypes respectively (1ng n=18, 2ng n=15). Similarly, nidogen1b morphants displayed 28% and 68% gross phenotypic response at 1ng and 2ng respectively (1ng n=29, 2ng n=25). Nidogen1a/1b morphants at 48hpf displayed gross morphological phenotypes in 45% and 59% of embryos examined at 1ng and 2ngs (1ng n=27, 2ng n=34)..

Nidogen2a^{-/-} embryos were injected with nidogen1a/b morpholinos in an attempt to inhibit function of the 3 nidogen orthologues expressed in the fissure. Reducing the function of three nidogen orthologues resulted in phenotypic characteristics not unlike those described in nidogen1a and 1b morphants (however in much higher numbers) and as such were categorized into the groupings previously described (Fig. 15, C.). Knocking down nidogen1a/1b in *nidogen2a*^{-/-} embryos at a concentration of .5ng resulted in an overwhelming percentage of embryos that displayed morphological phenotypes at 24hpf (95% in total). Knocking down nidogen1a/1b at concentrations of .75ng and 1ng also resulted in an extremely robust phenotypic response (100% and 99% respectively). The intense morphological response as a result of reduced nidogen1a, 1b and 2a function is likely due most embryonic tissues expressing one or more of these orthologues. As such,

knockdown of *nidogen1a*, *1b* and *2a* likely results in BM defects of multiple developing organ systems and subsequent perturbed gross morphological development.

Nidogen morphants display changes in eye size and shape

To determine whether the eye size and shape of *nidogen* morphant fish were significantly altered compared to controls at 24hpf, measurements were taken of both features (Fig. 16 A-E). At 24hpf *nidogen1a* morphant embryos displayed no significant difference in eye size at 1ng, however they displayed 16.07% smaller eyes with the 2ng treatment compared to controls ($p=.0086$). *Nidogen1b* morphant embryos displayed significantly smaller eyes at both 1ng and 2ng compared to control embryos (21% smaller, $p=.0001$ and 17% smaller, $p=.0034$ respectively). Finally, knock down of both *nidogen1a* and *1b* at 1ng and 2ng resulted in a significant, 14% and 25% decrease in eye size respectively, compared to controls ($p=.0034$ and $p=.0001$).

In addition to significantly smaller eyes, *nidogen* morphants displayed misshapen eyes compared to controls at 24hpf. *Nidogen1a* morphants at the 1ng concentration did not have a significantly misshapen eye compared to controls however, *Nidogen1a* morphant embryos at the 2ng treatment displayed a significant 15% elongation of the nasal/temporal axis of the eye ($p=.0001$). *Nidogen1b* morphants at 1ng displayed a significant 12% increase in the nasal-temporal length of the eye ($p=.0042$) however at the 2ng concentration the elongation was insignificant. Lastly, knockdown of *nidogen1a* and *1b* resulted in significantly elongated eyes at both 1ng and 2ng (18% elongation of the nasal temporal axis, $p=.0004$ and 24% elongation, $p=.0001$ respectively).

Preliminary measurements of eye size and shape were taken for *nidogen* morphants at 48hpf which yielded significantly smaller and elongated eyes compared to control morpholino in some treatment groups (Fig. 18). As shown in Figure 18 A, 48hpf *nidogen* morphant eyes are misshapen and less symmetrical compared to controls. Morpholino treatments that resulted in significantly elongated eyes at 48hpf include *nidogen1a* 2ng ($p=.0138$, $n=9$), *nidogen1b* 1ng ($p=.0176$, $n=15$), and *nidogen1a* and *1b* at 2ng ($p=.0017$, $n=8$). *Nidogen* morphant embryos also displayed smaller eyes at 48hpf compared to controls including 1ng *nidogen1b* ($p=.0011$, $n=15$) and *nidogen1a/1b* at 1

and 2ng ($p=.0001$ $n=12$ and $p=.0001$ $n=8$ for 1ng and 2ng respectively). These experiments need to be repeated to confirm these results.

Live imaging of nidogen morphant eyes reveals changes in eye development in real time

To capture the observed deviations of nidogen morphant eye development in real time, we conducted live imaging of nidogen1/1b morphants. Live imaging of nidogen1a/1b 2ng morphants from 18hpf to 36hpf revealed significant morphological alterations in eye development (Fig. 19). 2ng of nidogen1a/1b morpholinos were injected into RX3: GFP transgenic zebrafish embryos to visualize cells of the developing eye. Eyes of nidogen morphants at 18hpf were significantly smaller and elongated compared to WT controls and remained elongated throughout development until 36hpf. In addition to the elongated morphology of nidogen1a/1b morphant eyes, some RX3 expressing cells of morphant eyes lose contact and subsequently detach from the eye starting at 18hpf continuing to 36hpf (indicated by arrows). It is possible that decreased BM integrity as a result of reduced nidogen function, can cause cells of the eye to lose contact with the BM and ultimately become displaced. Following their displacement these cells will likely undergo anoikis and die and as a result be a factor in the microphthalmic phenotype observed in nidogen morphants.

Laminin deposition and basement membrane morphology is altered in nidogen morphants

Because knockdown of nidogen function resulted in readily observable gross morphological and eye phenotypes, we then wanted to directly examine the structure and the integrity of the BM of the eye. To do this, we observed the deposition of the ubiquitous BM component laminin as a proxy for the BM. IHC for laminin in nidogen morphant embryos revealed BM defects in the developing eye (Fig. 20). Specifically, laminin deposition in nidogen morphant eyes was less uniform and irregularly distributed

in the tissues of the developing eye compared to controls. Embryos with more severe gross morphological phenotypes (indicated by colored box representing category of gross morphological phenotype in Fig. 15) displayed more robust laminin deposition defects compared to WT and mildly effected morphants. It is likely that the absence of nidogens, which enable crosslinking laminin and collagenIV networks, results in reduced BM integrity and the displacement of its components. It may also be the case that the reduction of BM biomechanical strength in nidogen morphants results in the inability of the BM to properly provide the structural framework of the developing eye resulting in the observed elongated morphology.

Eye patterning gene expression is altered in nidogen morphants

After observing that reducing nidogen function leads to smaller and elongated eyes, likely as a result of BM defects, we then wanted to determine whether these morphological changes alter expression of genes involved in retinal patterning. Aside from playing a structural role, BMs have been shown to utilize multiple signaling pathways and mechanisms to relay vital information to the cells in which they support both in development and pathogenic scenarios (Harburger and Calderwood 2009, Smith et al. 2007, Maranti and Brugge 2002). Because of this, we believed it wholly possible that disruption BM integrity via the knockdown of nidogen may lead to changes in the expression of genes involved in the early patterning of the eye.

To examine how disruption of BM integrity through loss of nidogen effects retinal patterning, we conducted whole mount *in situ* hybridization for genes whose expression domains are confined to specific areas of the developing eye in both *nid1a/1b* morphants and WT embryos (Fig. 21). Specifically, we have examined the expression profiles of dorsal, ventral, temporal, and nasal patterning regulators, *Aldh1a2*, *Vax2*, *Foxg1a* and *FoxD1* at 24hpf respectively (Fig. 21, B). Notably, the expression pattern of the dorsal regulator *Aldh1a2* shifts toward the nasal axis in *nid1a/1b* morphants (Fig. 21 a7-a8 and c7-c8). Moreover, the ventral regulator *Vax2*'s expression increases and is located ectopically of the developing retina in *nid1a/1b* morphants (Fig. 21 a6-a6 and c5-c6).

The instance of Vax2 overexpression may be explained by previously observed downregulation of BM mediated BMP signaling in nidogen mutants (Bose et al. 2006). Specifically, it has been shown that BMP4 suppresses Vax2 expression in the developing eye (Hasagawa et al. 2016). Together, these data suggest that downregulated BMP signaling in the eye as a result of nidogen removal and subsequent disrupted BM integrity may lead to an increase in Vax2 expression.

Reducing nidogen function with a dominant negative construct

To reduce the function of endogenous nidogen and confirm our morpholino results, we generated a dominant negative nidogen1b construct. mRNA generated for this construct contained sequence for nidogen1b devoid of its G3 domain. Ultimately, when expressed, this dominant negative version of nidogen would bind to laminin, however it would not have the ability to bind to collagenIV. We predict that this nidogen variant will saturate laminin's endogenous nidogen binding sites therefore decreasing endogenous nidogen's ability to link the collagenIV and laminin networks.

To introduce the dominant negative nidogen1b we injected embryos with mRNA and performed laminin IHC to examine BM characteristics (Fig. 22). Embryos were injected with 200pg, 300pg, and 350pg of dominant negative nidogen1b mRNA and embryos displaying disrupted eye development at 24hpf were recorded. The number of embryos displaying morphological phenotypes as a result of dominant negative nidogen1b mRNA injection occurred in a dose dependent manner. At 200pg, 21% of embryos displayed defects in eye shape (Fig. 22 B and C). At 300pg and 350pg 60% and 77% of dominant negative nidogen1b embryos displayed misshapen eyes at 24hpf. IHC for laminin showed laminin deposition was comparable to controls in eyes of embryos injected with dominant negative nidogen1b mRNA (Fig. 22, B). This may indicate that reduction of nidogen1b function by introducing dominant negative nidogen is less impactful than the use of nidogen morpholinos. However, the resulting aberrations of retinal morphology suggest dominant negative nidogen does in some way alter BM integrity and subsequent eye development in a similar fashion to nidogen morpholinos.

Generating a Nidogen1b dominant negative conditional mutant to target ESF

To target and assess nidogen's contribution to the stability of the BM in the CF specifically, we have designed and implemented Tol2 Transgenesis. (Kwan et al. 2007) We have designed constructs to drive the expression of dominant negative nidogen1b via the *hsp70* heatshock promoter which can be turned on during key ESF events. We have generated preliminary results showing the dominant negative nidogen1b construct responds to heatshock to produce mRNA *in vivo*. WISH was conducted for nidogen1b in 24hpf injected embryos following heat shock (Fig. 23). The resulting mosaic pattern of gene expression is indicative of production of dominant negative nidogen1b mRNA. Injected embryos are currently being raised to generate transgenic lines.

It is the goal of this experiment to, by driving the expression of dominant negative nidogen, determine if we can directly affect ESF in the choroid fissure. For example, by driving the expression of dominant negative nidogen prior to BM breakdown within the choroid fissure, it may be possible to prematurely reduce BM integrity. It would be interesting to observe that if reducing BM strength in turn provides the physical cues to trigger ESF. If this is the case, it may be possible to 'jumpstart' ESF within the choroid fissure prior to its proper timing by simply altering nidogen function. These data may provide more evidence that nidogen's relationship to BM structure is a key component of BM remodeling prior to ESF.

Table 2. Nidogen amino acid and nucleotide percent identity matrices.

A

Amino Acid % Identity Matrix				
	nidogen1a	nidogen1b	nidogen2a	nidogen2b
nidogen1a	100.00	58.72	40.50	39.07
nidogen1b	58.72	100.00	40.45	38.57
nidogen2a	40.50	40.45	100.00	51.39
nidogen2b	39.07	38.57	51.39	100.00


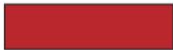
B

Nucleotide % Identity Matrix				
	nidogen1a	nidogen1b	nidogen2a	nidogen2b
nidogen1a	100.00	63.99	52.14	49.39
nidogen1b	63.99	100.00	53.12	48.66
nidogen2a	52.14	53.12	100.00	61.64
nidogen2b	49.39	48.66	61.64	100.00

Identity matrices were generated using Clustal Omega's multiple sequence online alignment tool. **A)** Amino acid identity matrix for all four nidogen orthologues. Nidogen1a and nidogen1b share the highest sequence identity at 58.74%. Nidogen2a and nidogen2b are the second highest sequence identity at 51.39%. **B)** nucleotide identity matrix for all four nidogen orthologues. Nidogen1a and nidogen1b share the highest sequence identity at 63.99% and nidogen2a and nidogen2b share the second highest at 61.64%.

Table 3. A summary of the expression of all major BM components detected in the choroid fissure of the developing eye.

Gene	24hpf	32hpf	48hpf	56hpf	65hpf
nidogen1a	Green	Green	Red	Red	Red
nidogen1b	Green	Green	Green	Green	Red
nidogen2a	Green	Green	Green	Red	Red
nidogen2b	Red	Red	Red	Red	Red
laminina1	Green	Green	Green	Green	Red
laminina4	Green	Green	Green	Red	Red
lamininc1	Green	Green	Green	Green	Red
collagen4a1	Green	Green	Green	Green	Green
collagen4a2	Green	Green	Green	Green	Green
perlecan	Green	Green	Green	Green	Green

 Gene expression detected in choroid fissure
 Gene expression not detectable in choroid fissure

Green boxes indicate that there is observable expression within the choroid fissure while red boxes indicate no detectable expression. The expression of *nidogen 1a* is the first gene to become undetectable within the choroid fissure at 48hpf. The expression of *nidogen1b* is last detected at 56hpf and the expression of *nidogen2a* is last detected at 48hpf. Of the three laminin genes examined *laminina1* and *lamininc1* become last detected at 56hpf and are expressed longer than both *nidogen1a* and *nidogen2a*. Interestingly, the expression of the *collagens* (*4a1* and *4a2*) and *perlecan*, remains detectable within the choroid fissure even at 65hpf and are detectable for the longest duration. Of the 10 genes examined two of the three *nidogen* genes expressed within the choroid fissure become undetectable earlier than *perlecan*, both *collagen4s*, and two of the three *laminins*.

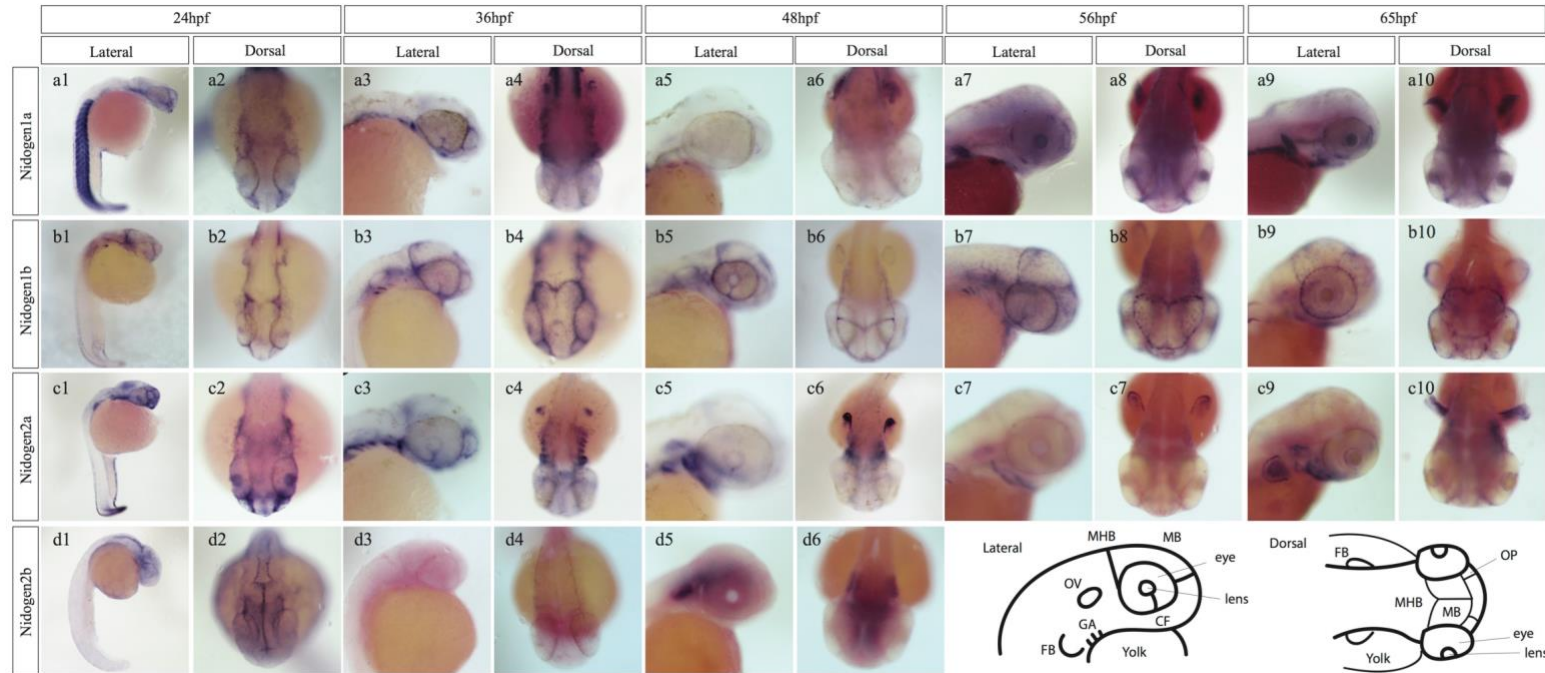


Figure 6. WISH for all four *nidogen* orthologues from 24-65hpf

WISH analysis for all four zebrafish *nidogen* orthologues has revealed both overlapping and unique areas of expression from 24-65hpf across orthologues. All are representative images. At 24hpf, the expression of *nidogen1a* is most prominent in the developing somites (a1) and dorsally can be observed within the olfactory placode (OP), outlining the midbrain regions (MHB), and within the tissues surrounding the eyes including the choroid fissure (a2). At 36hpf the expression of *nidogen1a* remains consistent and can now be prominently observed in the choroid fissure and developing gill arches (GA) (a3 and a4). At 48hpf expression of *nidogen1a* decreases dramatically in the head but can still be observed in the developing fin bud (FB)(a6). At 56hpf and 65hpf *nidogen1a* is expressed in the lens (a7 and a9), and prominently in the fin buds (a8 and a10). At 24hpf *nidogen1b* expression was observed in the tissues outlining the tail (b1), and like *nidogen1a*, outlining the midbrain regions (MHB), and within the tissues surrounding the eyes (b2). In addition to the tissues described at 24hpf, at 36hpf *nidogen1b* expression was observed in tissues outlining the otic vesicle (OV) (b3). From 48hpf to 65hpf *nidogen1b* expression was observed in tissues outlining the mesencephalon (M), the eye including the choroid fissure (until 56hpf), and fin buds (b6-b10). *Nidogen2a* expression at 24hpf is most prominent at the distal tip of the tail (c1), strongly in the head (c1 and c2) and within the lens (c2). From 36hpf to 65hpf like *nidogen1a*, *nidogen2a* expression can be seen in the developing gill arches, and the developing fin buds (c3-c10). Expression of *nidogen2a* was observed in the eye until 48hpf (c5). Unlike its counterparts, at 24hpf expression of *nidogen2b* is not observed in the tail (d1) but is observed in the head specifically down the midline spanning the fore and midbrain and in throughout the hindbrain ventricle (d2). Expression of *nidogen2b* at 36hpf is virtually nonexistent but is later expressed in the otic vesicle at 48hpf (d5 and d6).

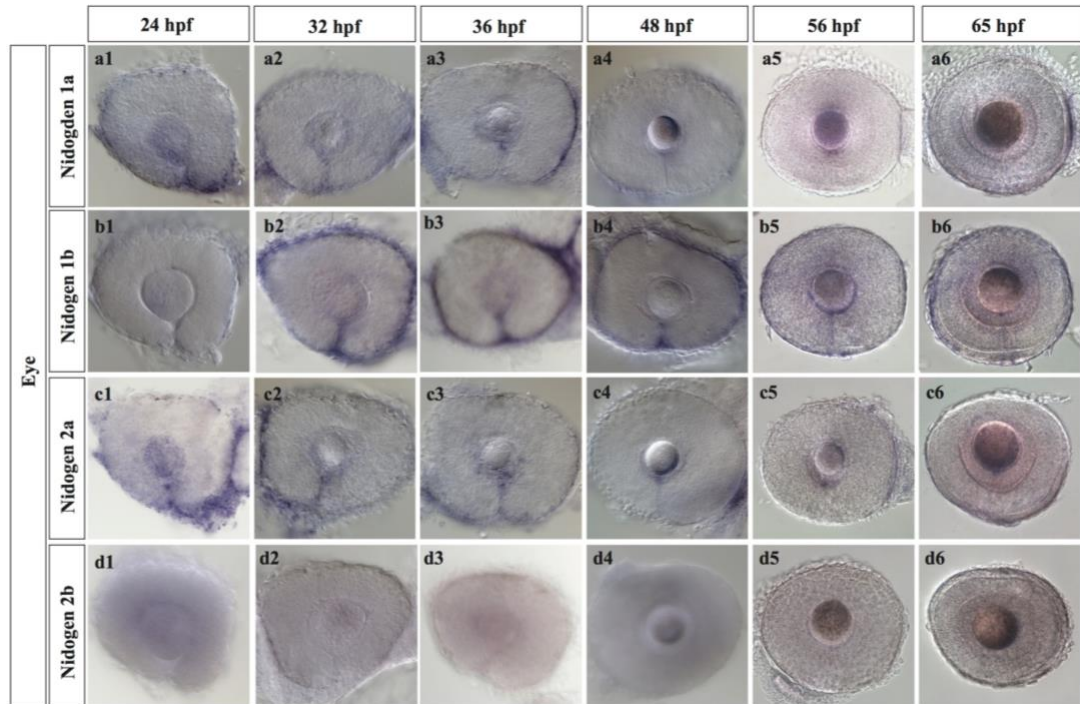


Figure 7. WISH for all four nidogen orthologues from 24-65hpf- dissected eyes

Representative images of WISH analysis on dissected eyes conducted for all four *nidogen* orthologues. WISH showed *nidogen1a*, *1b*, and *2a* to be expressed in the developing eye specifically within the region of the choroid fissure while *nidogen2b* was not detected (a2, b2, c2 and d1-d6). The expression of *nidogen1a* is last detected within the choroid fissure at 36hpf (a3). *Nidogen1b*'s expression within the choroid fissure is observable until 56hpf (b5). The expression of *nidogen2a* is observable within the choroid fissure until 48hpf (c4). There was no detectable expression of any *nidogen* orthologues within the choroid fissure at 65hpf (a6-d6).

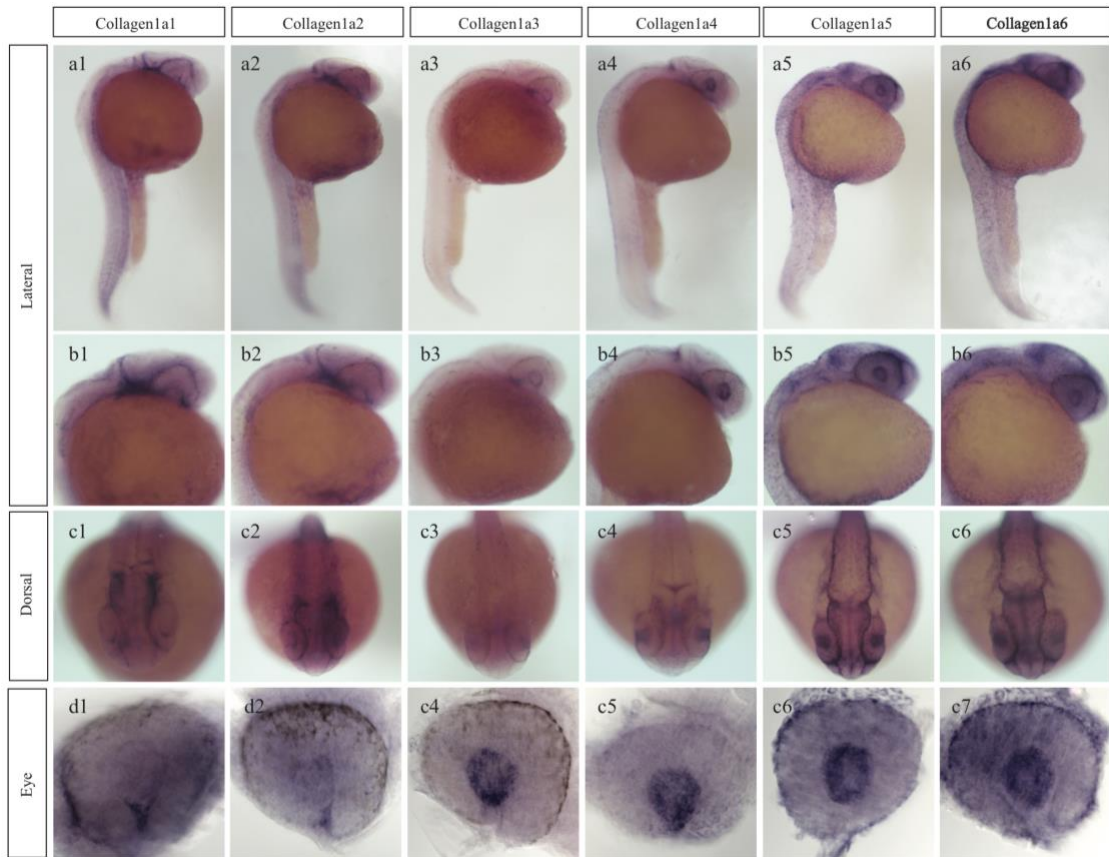


Figure 8. WISH for all collagen4 genes examined at 24hpf

The expression patterns of six *collagenIV* genes were analyzed in zebrafish embryos at 24hpf to determine which orthologues were expressed in the choroid fissure. From the data above, it was determined that *collagen4a1* and *collagen4a2* would be examined at later time points because of their expression within the choroid fissure (d1 and d2).

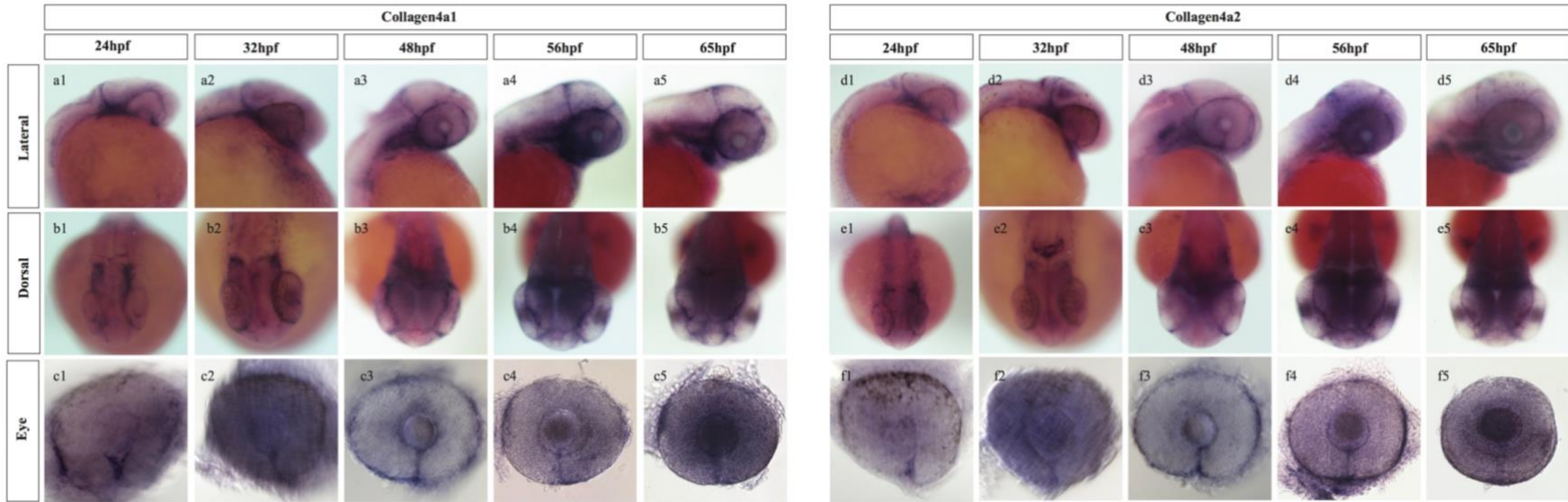


Figure 9. WISH for collagen4a1 and collagen4a2 from 24-65hpf

The expression of both *collagen4a1* and *collagen4a2* was observed in the choroid fissure from 24-65hpf (c1-c5 and f1-f5). Laterally, *collagen4a1* was observed at the mid-hindbrain at 24-48hpf (a1-a2). At 56 and 65hpf, *collagen4a1* expression was observed both at the mid-hindbrain boundary and at the boundary of the forebrain and the midbrain (a4-a5). Similarly, the expression of *collagen4a2* was observed at the mid-hindbrain boundary at 24-48hpf (d1-d3) and later also in the tissues separating the fore and midbrain (d4-d5). Expression of both *collagens* was also observed in the developing gill arches from 24-56hpf (a1-a5 and d1-d5). Additionally, at later time points (56hpf and 65hpf) *collagen4a1* and *a2* expression was detected in the developing fin buds (b4-b5, and e4-e5).

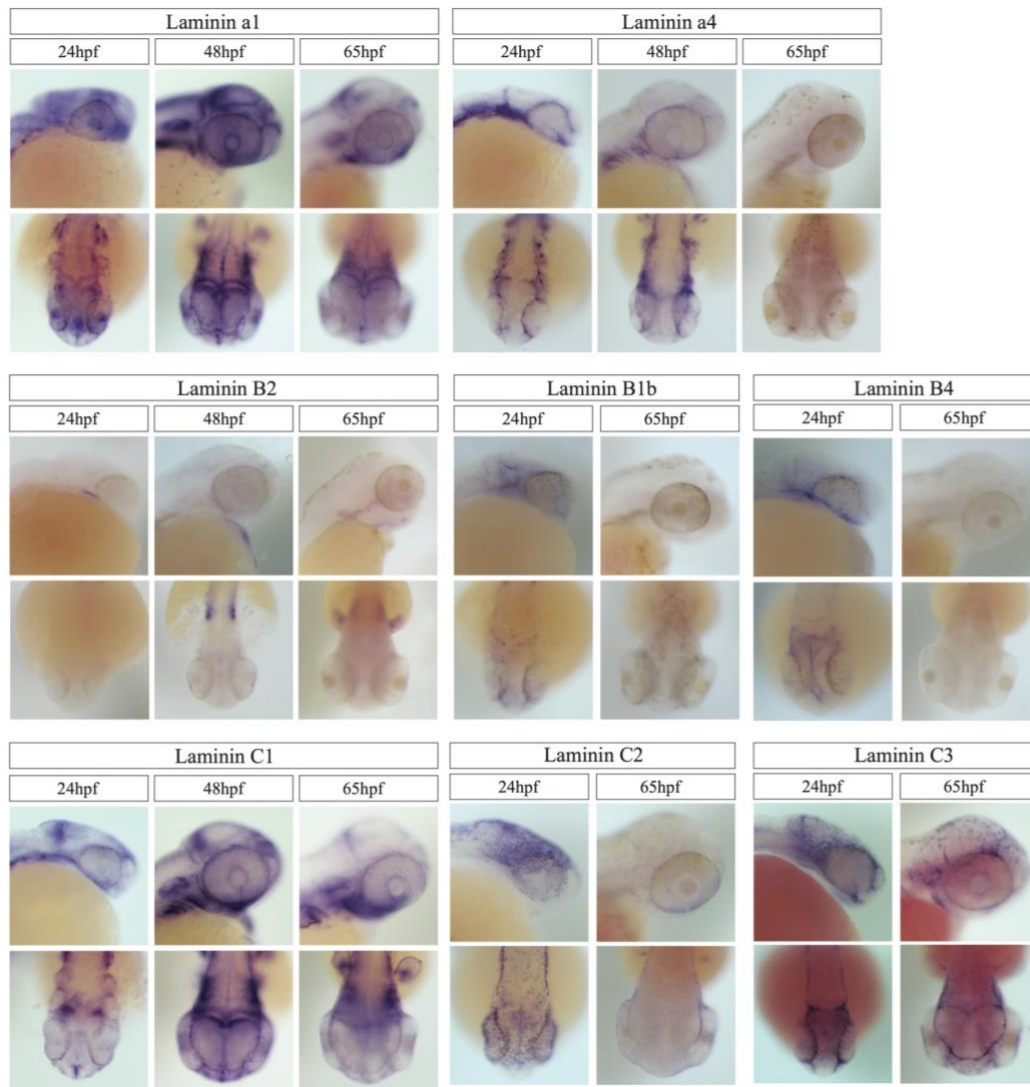


Figure 10. WISH analysis for all laminin genes examined

Lateral and dorsal expression profiles were examined for eight zebrafish *laminin* genes. From these data it was determined the expression of *laminin a1*, *laminin a2* and *laminin c1* were expressed within the choroid fissure (top row and bottom row first panel) and a more complete expression profile was generated for these genes (Fig. 11)

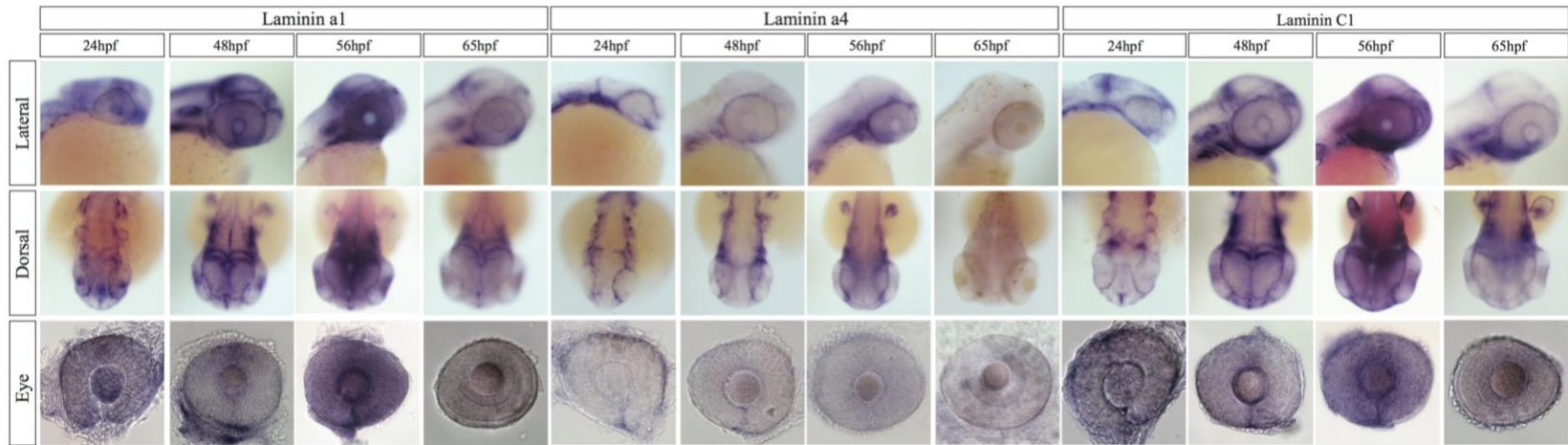


Figure 11. WISH for laminin a1, laminin a4 and laminin c1 from 24-65hpf

WISH analysis was conducted from 24hpf to 65hpf for *laminin a1*, *laminin a4* and *laminin c1* all of which were determined to be expressed within the choroid fissure. All are representative images. *Laminin a1* is expressed in the head of the embryo from 24hpf-65hpf outlining the mesencephalon, the metencephalon the diencephalic ventricle, the otic vesicle, and the developing fin buds (a1-a8). In the eye, *laminin a1* expression was observed in the choroid fissure until 56hpf (a9-a11). *Laminin a4* expression was observed from 24hpf to 56hpf in the head of the embryo surrounding the developing eye, the gill arches, and the developing limb buds. In the eye, *laminin a4* expression was last detected within the choroid fissure at 48hpf (b9-b12). *Laminin a4* expression was not observed in any tissues at 65hpf (b4, b8 and b12). *Laminin c1* expression is similar to that of *laminin a1* from 24hpf-65hpf. *Laminin c1* was detected outlining the mesencephalon, the metencephalon the diencephalic ventricle, the otic vesicle, the developing fin buds, and the gill arches (c1-c8). In the eye *laminin c1* expression was last detected at 56hpf (c9-c12).

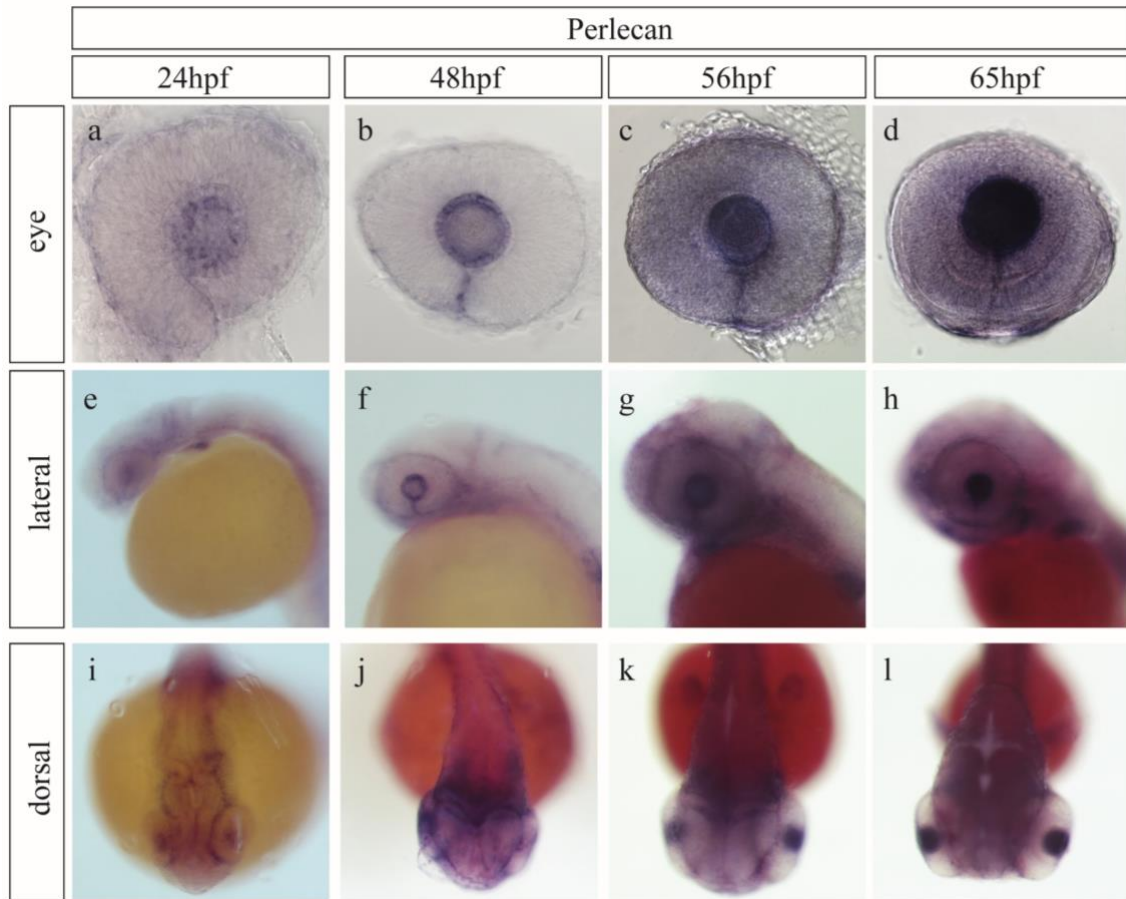


Figure 12. WISH for perlecan from 24-65hpf

Wish for *perlecan* revealed *perlecan* expression in the developing choroid fissure from 24 to 65hpf (a-d). Additionally, *perlecan* expression was observed in tissues surrounding and of the developing lens from 24-65hpf (a-d). At 24hpf *perlecan* expression was observed surrounding regions of the brain including the mesencephalon, the midbrain and the hindbrain (i) and was observed surrounding the tissues of the brain at later time points (j-l). Laterally, *perlecan* expression was observed at the mid-hindbrain boundary from 24hpf-65 hpf (e-g). Additionally, *perlecan* expression was observed in the developing fin buds at 56hpf and 65hpf (k and l).

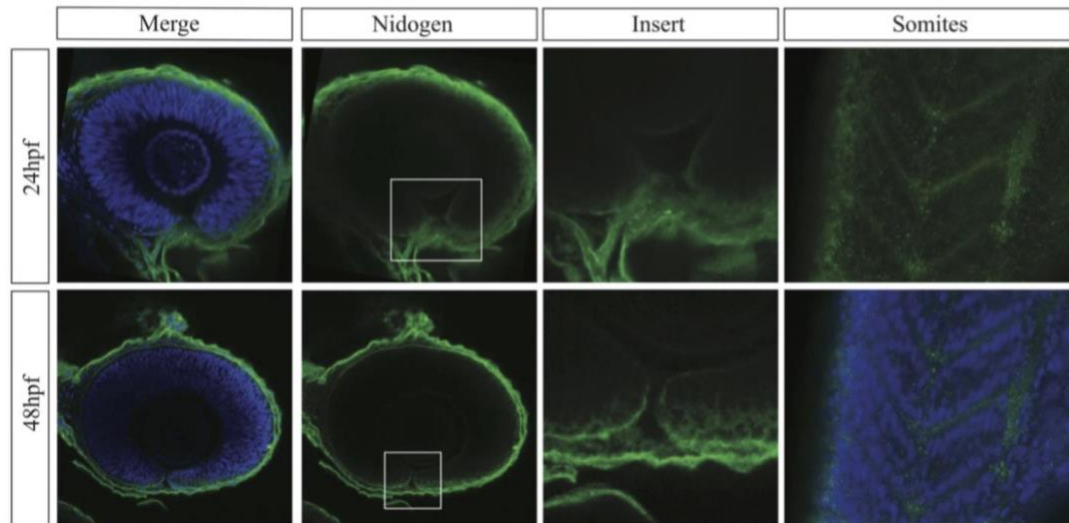


Figure 13. IHC for nidogen in the zebrafish eye at 24 and 48hpf.

A whole mount IHC analysis, utilizing rabbit α -nidogen1/2 confirmed the deposition of nidogen to the basement membrane of the developing zebrafish eye (green). At both 24hpf and 48hpf nidogen was observed to be deposited in the basement membrane surrounding the lobes of the developing eye (white box and inset). Additionally, nidogen signal was observed in the basement membrane surrounding the developing somites at 24hpf.

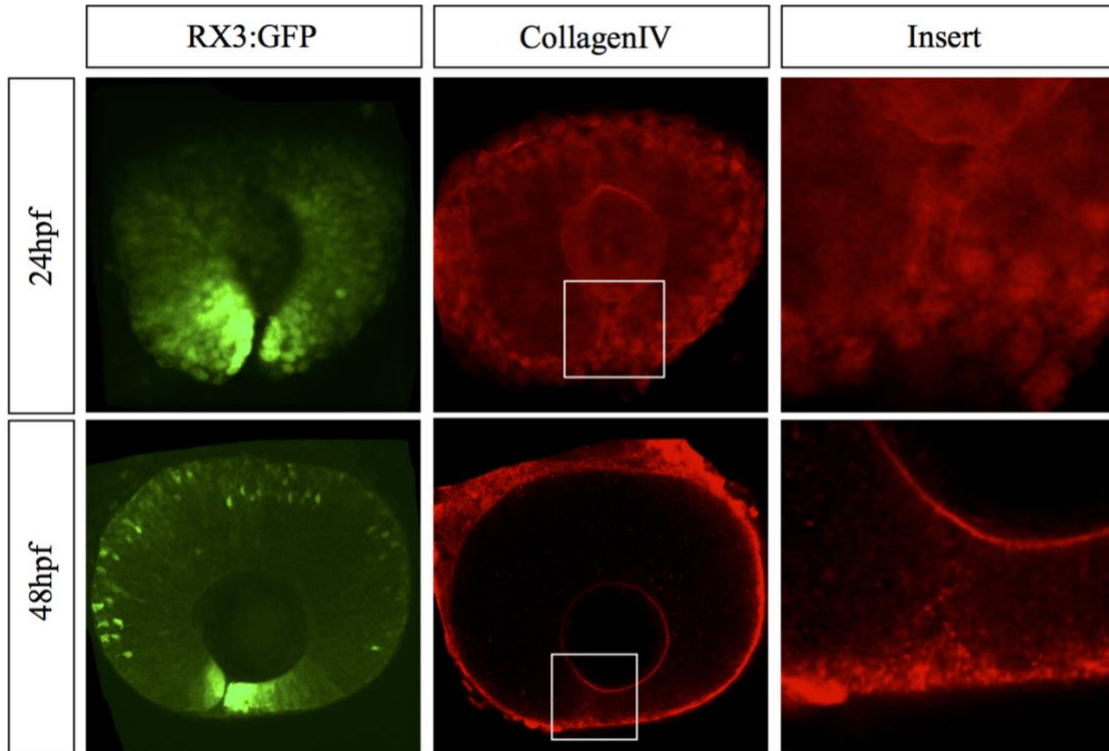


Figure 14. IHC for collagenIV in the developing zebrafish eye at 24 and 48hpf

Anti-rabbit collagenIV was used to observe the deposition in the of collagenIV in the developing zebrafish eye (b and f) (red). Green indicates RX3:GFP expression indicating cells of the developing eye (a and e). CollagenIV deposition was observed surrounding the tissues of the eye (b and f) and in the tissues surrounding the lobes of the eye (c and g) at 24 and 48hpf.

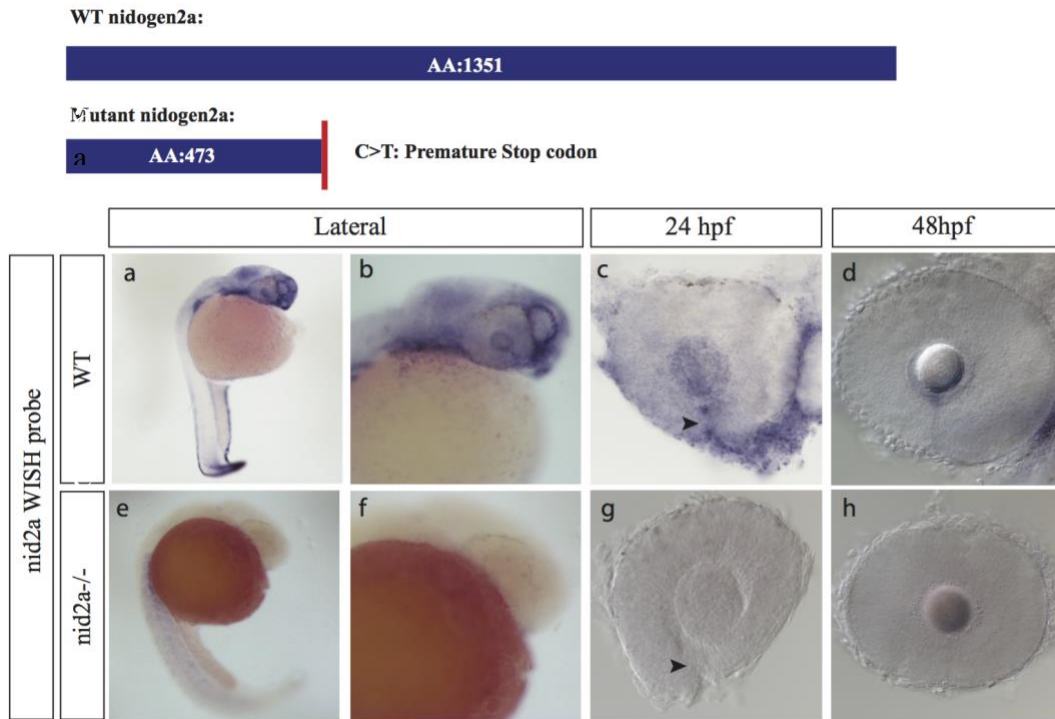


Figure 15. Nonsense mediated decay detected in nidogen2a mutants

A) A schematic representation of WT and nidogen2a mutant transcripts. The mutant nidogen2a transcript has a C>T mutation resulting in a severely truncated and non-function protein. **B)** WISH conducted for nid2a transcripts in nidogen2a null mutants shows little to no signal. Expression of nid2a in WT embryos (a-b) shows specific expression in both the choroid fissure at 24 and 48hpf (c and d) and at the tip of the tail at 24hpf (a/ arrow). In confirmed nidogen2a homozygous mutants no expression was detected in the developing eye (g and h) or at the tip of the developing tail (e/ arrow).

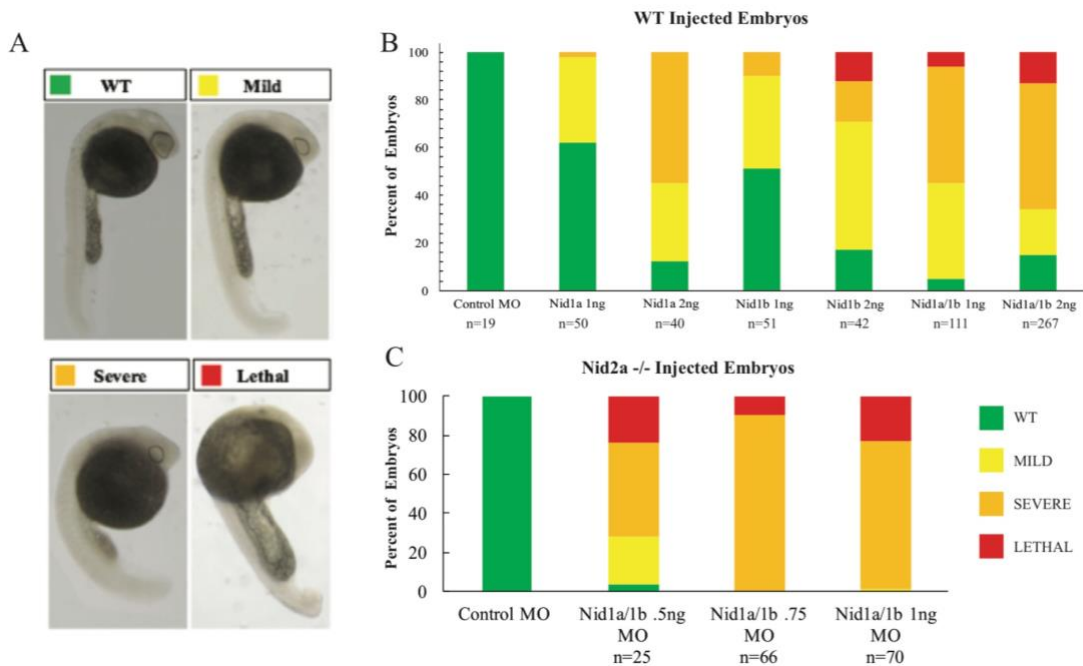


Figure 16. Nidogen morpholino analysis at 24hpf- gross morphology

A) Representative images of phenotypic categorizations of nidogen morphants from WT to lethal each with a corresponding color for identification in graphs B and C. Morphants categorized as WT (green) were undistinguishable from uninjected or control morphant embryos. Embryos categorized as mild (yellow) had a slight curvature of the tail, a slightly elongated eye (nasal/temporal axis), and mild cloudiness in regions of the brain. Severe morphant embryos (red) had a robust curvature of the tail, a markedly smaller eye, and readily observable cloudiness and indistinguishable brain features. Lethal morphant embryos were categorized as any phenotypic response more robust than severe. **B)** Percentage of embryos displaying each phenotypic categorization for each morpholino treatment injected into AB embryos. Nidogen1a and nidogen1b morpholinos were injected independently and together at 1ng and 2ng concentrations. **C)** Percentage of embryos displaying each phenotypic categorization for each morpholino treatment injected into *nidogen2a* homozygous mutants.

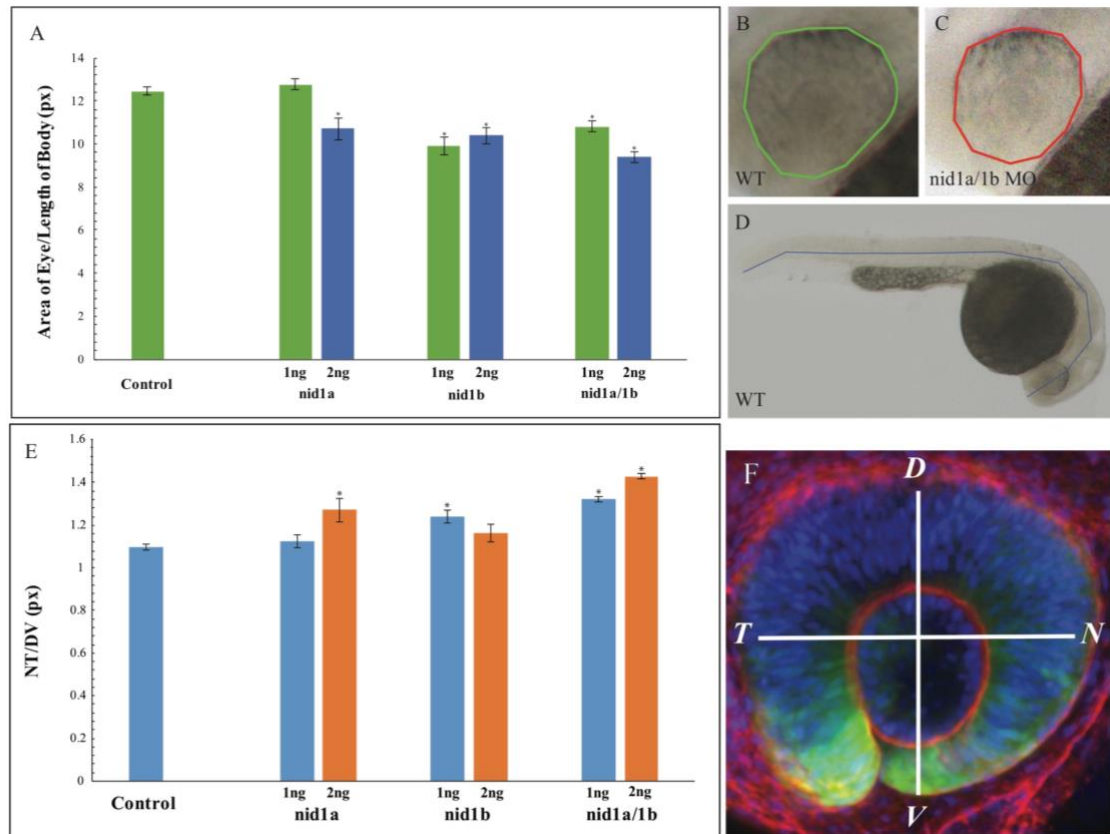


Figure 17. Nidogen morpholino analysis at 24hpf- eye size and eye shape

Nidogen morphant embryos display smaller and elongated eyes compared to WT controls following a dose response at 24hpf. **A)** Nidogen1a MO at 2ng resulted in significantly smaller eyes (16.6%, $p=.0086$) compared to controls ($n=21$). Both nidogen1b treatments (1ng, $n=21$ and 2ng, $n=18$) resulted in significantly smaller eyes compared to controls at 24hpf (20.7%, $p=.0001$ and 16.7%, $p=.0034$ respectively). Injections of nidogen1a and 1b MO together produced significantly smaller eyes at both 1ng (13.34%, $p=.0034$, $n=43$) and 2ng (24.48%, $p=.0001$, $n=28$) concentrations. **B-D)** is a schematic representation of how measurements of eye sizes were taken. **B** and **C** show outlines of embryonic eyes at 24hpf for WT and nidogen1a/1b respectively. The area (px) of these eyes were analyzed as a factor of the length (px) of the embryo from tip to tail (**D**). In addition to smaller eyes, eyes of nidogen morphant embryos displayed an elongation of the nasal temporal axis. **E)** Elongation of the nasal-temporal axis of the eye followed a dose dependent response in both single and double morphant fish at 24hpf. Eye shape was determined as in panel **F** by measuring the nasal-temporal axis (px) in a ratio with the dorsal temporal axis (px). Nidogen1a MO treatments at 1ng did not result in significant changes in eye shape ($p=.3279$), but at 2ng produced significantly elongated eyes, (15%, $p=.0001$, $n=17$). Injection of nidogen1b MO at 1ng resulted in a significant 12% elongation ($p=.0042$, $n=22$) however at 2ng did not produce significant results ($p=.3364$). Injection of both MOs resulted in significantly elongated eyes at both 1ng (17.7%, $p=.0004$, $n=43$) and 2ng (26%, $p=.0001$, $n=28$).

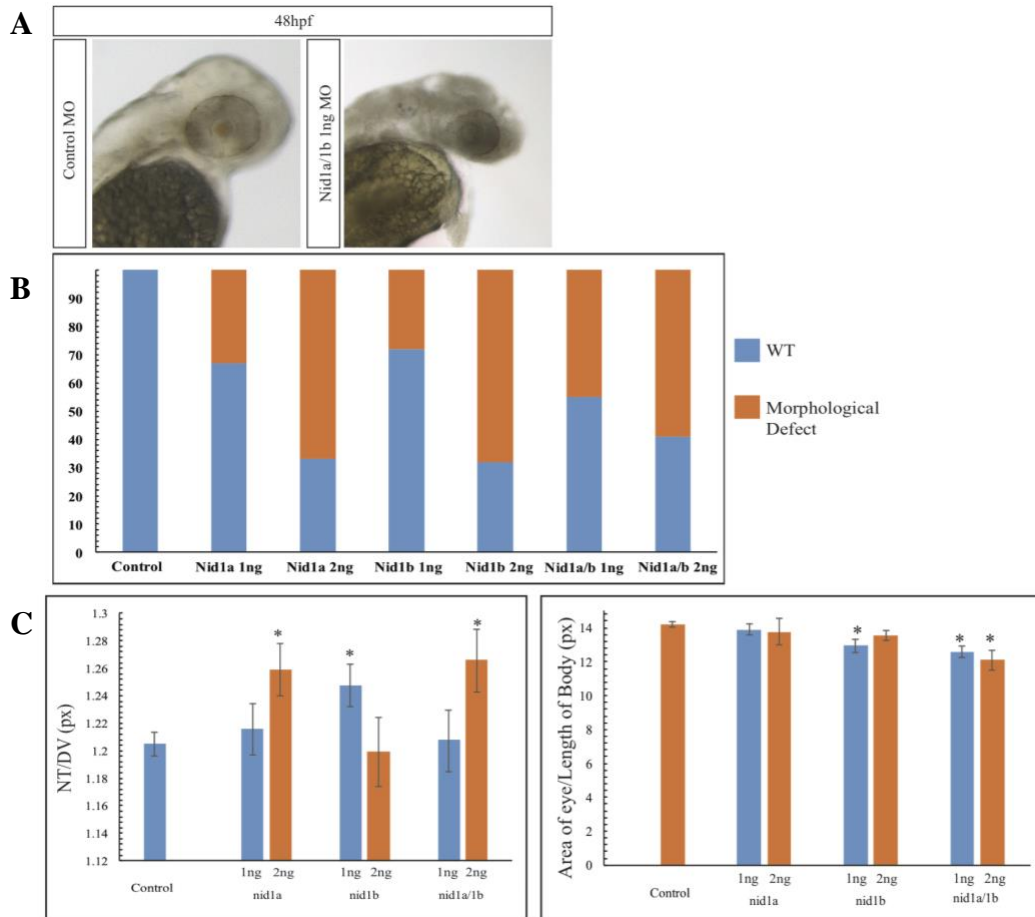


Figure 18. Nidogen morpholino analysis at 48hpf

A) representative images of 48hpf embryos from both control morpholino and *nidogen1a/1b* morpholino treatments. **B)** percentages of embryos from each treatment group displaying aberrant gross morphological phenotypes such as those depicted in A. Notably, embryos displaying gross morphological phenotypes followed a dose response for both *nidogen1a* and *nidogen1b* morpholinos independently and together. **C)** Measurements of eye size and shape were determined as in figure 17. Some treatment groups displayed significantly elongated eyes at 48hpf including *nidogen1a* 2ng ($p=.0138$, $n=9$), *nidogen1b* 1ng ($p=.0176$, $n=15$), and *nidogen1a* and 1b at 2ng ($p=.0017$, $n=8$). *Nidogen* morphant embryos also displayed smaller eyes at 48hpf compared to controls. These include 1ng *nidogen1b* ($p=.0011$, $n=15$) and *nidogen1a/1b* at 1 and 2ng ($p=.0001$ $n=12$ and $p=.0001$ $n=8$ for 1ng and 2ng respectively).

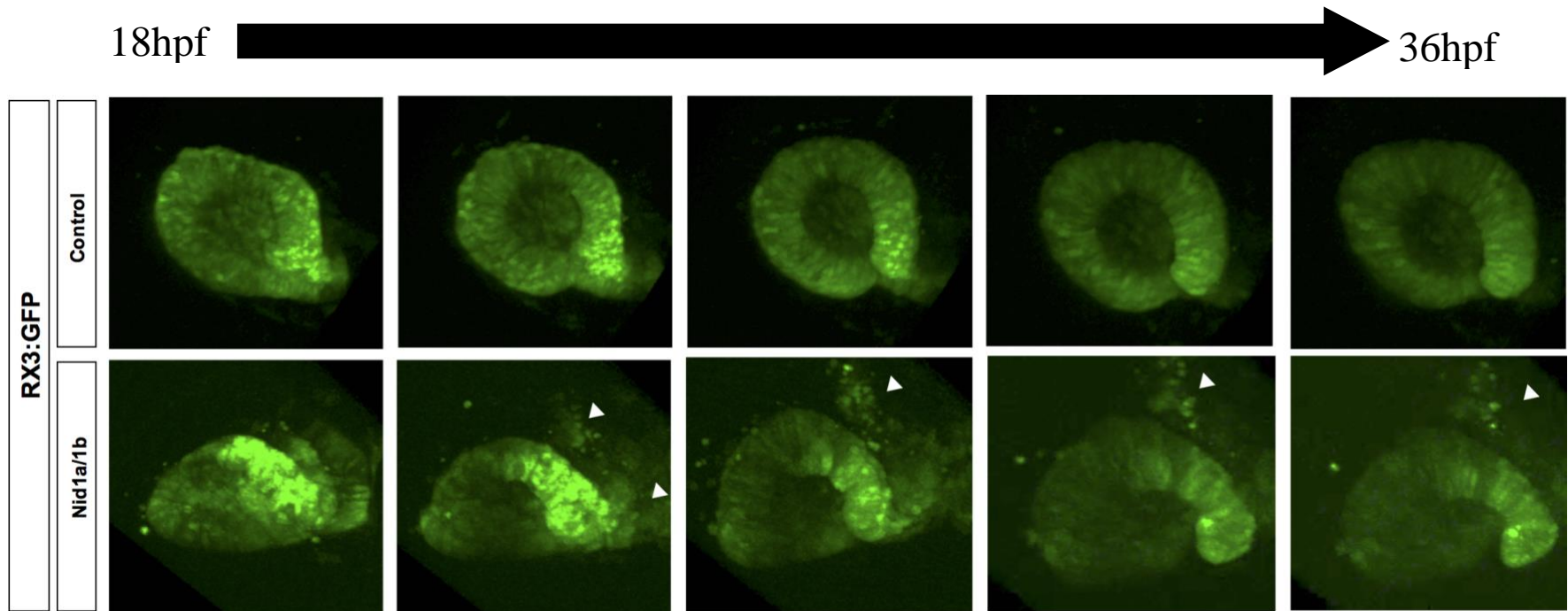


Figure 19. Live imaging of *nid1a/1b* double morphants from 18hpf to 36hpf

Live imaging of *nidogen1a/1b* double morphants shows morphological abnormalities in the developing eye from 18hpf to 36hpf. Arrows depict cells detached from the basement membrane.

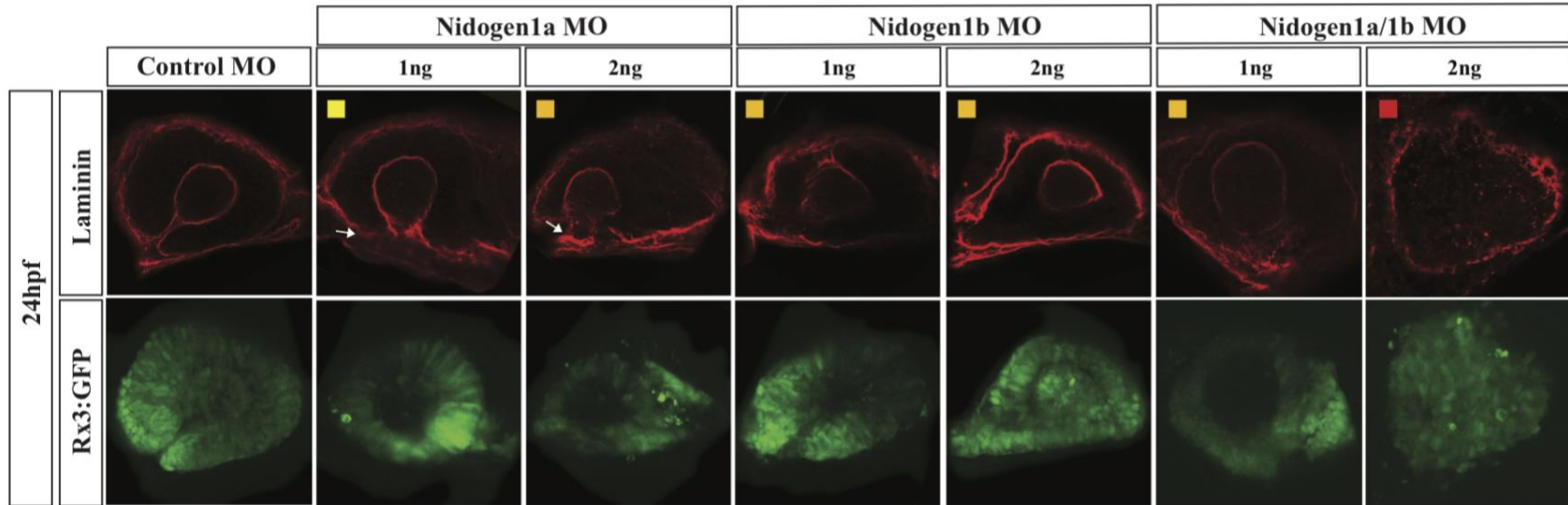


Figure 20. IHC analysis of laminin deposition in nidogen morphant embryos

Immunohistochemical analysis of laminin (red) in nidogen morphant eyes show deposition abnormalities. Colored boxes indicate representative images of eyes from gross morphological categorizations previously described and depicted in Fig. 16. Green indicates RX3:GFP expression and thereby cells of the developing eye. The overall eye laminin distribution in nidogen morphants is disrupted and not as uniform compared to controls. Elongation of the developing eye is also easily observable in severe nidogen morphant phenotypes. Nid1a morphants show irregular laminin deposition specifically in the region of the choroid fissure (arrows).

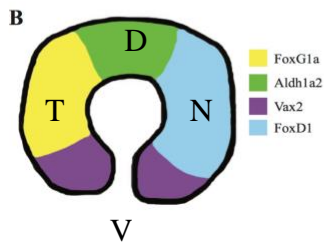
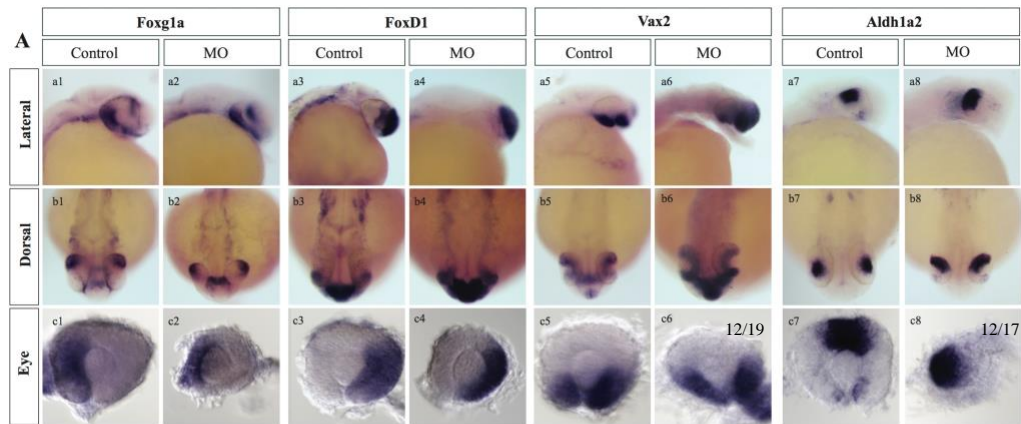


Figure 21. Whole mount *in situ* hybridization in *nidogen1a/1b* morphants and WT embryos of genes involved in eye patterning

A) WISH Gene expression profiles for genes involved in eye patterning in both control MO and *nid1a/1b* 2ng MO embryos. Dissected eyes from both control and morphant embryos and imaged for analysis (e1-e8). *Vax2* gene expression in *nidogen1a/1b* morphant embryos increases (n=12/19) (a5 and a6, c5 and c6) *Aldh1a2* expression shifts from the most dorsal part of the eye temporally (n=12/17) (a7 and a8, e7 and e8). **B)** a schematic representation of genes involved in the patterning of the zebrafish eye at 24hpf (NTDV depicts nasal, temporal, dorsal, ventral). These data suggest that *nidogen* removal from the basement membrane can alter the expression of patterning genes within the developing eye.

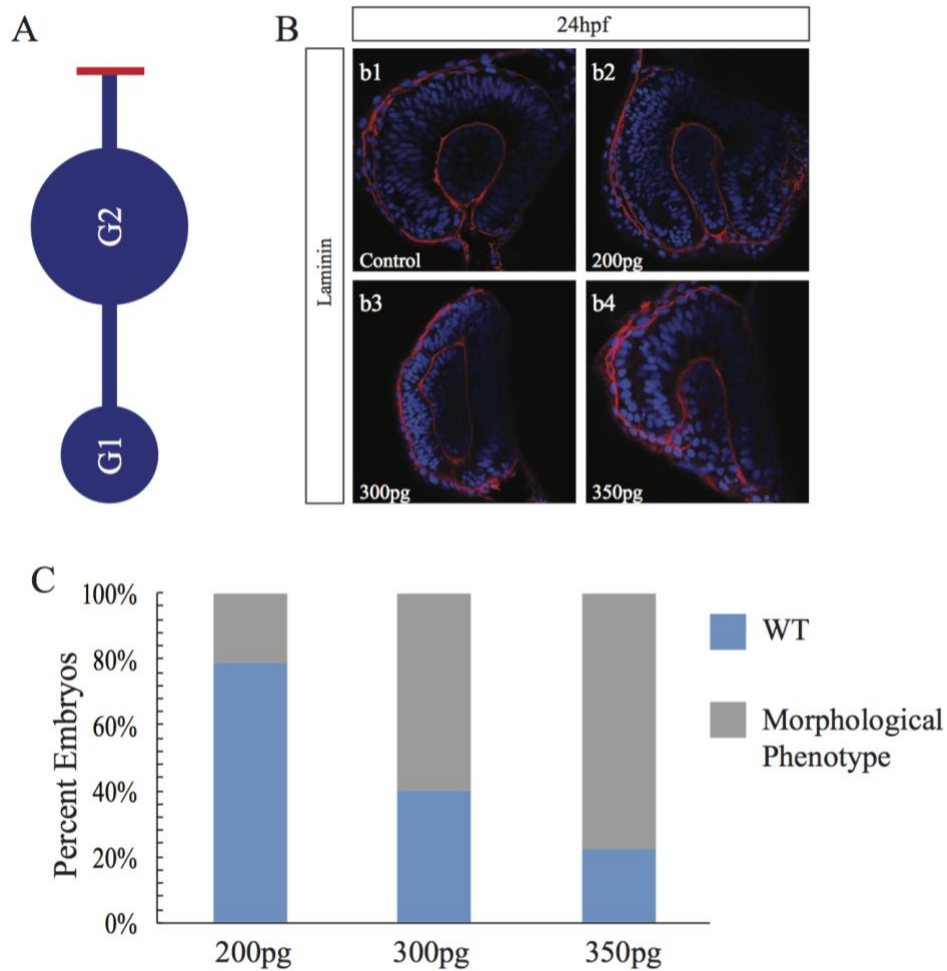


Figure 22. Dominant Negative Nidogen1b Phenotypes

A) a schematic representation of dominant negative nidogen1b protein structure. The transgenic nidogen protein still has the G1 and G2 domain, but lacks the G3 domain. This results in the protein having the ability to interact with laminin but not collagenIV thereby disrupting BM architecture. **B)** Dominant negative nidogen expressing embryos displayed irregular morphology of the developing eye, specifically in the region of the CF at 24 hpf at all three concentrations injected (b2-b4). **C)** ratios of morphological observed followed a dose response from 200pg to 350pg with increasing concentrations of injected DN mRNA.

A



B

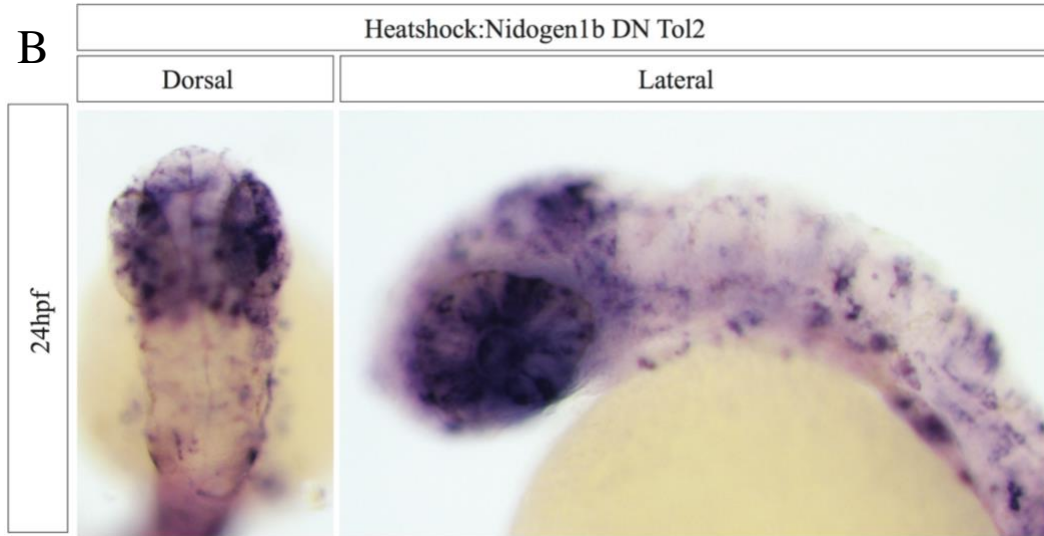


Figure 23. WISH for *nidogen1b* in transgenic dominant negative *nidogen1b* embryos after heat shock.

A) a schematic of the Tol2 dominant negative *nidogen1b* construct. B) WISH was performed for *nidogen1b* in Tol2 dominant negative *nidogen1b* embryos after heat shock at 24hpf. The resulting mosaic expression pattern is indicative of transgene insertion into the embryonic genome.

CHAPTER FOUR

DISCUSSION

The remodeling and removal of the BM within the CF prior to ESF is undoubted, however the underlying mechanisms governing this process remain unknown. It is likely the case that a dynamic interplay exists between gene expression of BM components and protein level protease interactions that ultimately result in the disassembly and removal of the BM within the CF. The data presented in this thesis provides evidence that regulation of nidogen may play a key role in compromising BM integrity ultimately leading to its removal to allow for subsequent ESF.

In concurrence with my hypothesis, I have shown that nidogen is required for BM integrity. Specifically, limiting nidogen deposition in the zebrafish embryonic model via the use of morpholinos has resulted in compromised BM structure via the disruption of ternary complexes and phenotypes similar to those observed in the murine model. *Nidogen1a* and *1b* knockout mice have been shown to display BM defects in the heart, lung, and limbs resulting in perinatal lethality (Bader et al. 2005 and Bose et al. 2006). These defects were observed to be a direct result of weakened BM integrity due to a decrease in the deposition of laminin, perlecan, and collagenIV. Additionally, knockout of *nidogen 1* in mice has been reported to decrease the deposition of laminin y1 resulting in a more punctate and less uniform BM compared to controls (Baranowsky et al. 2010). Examined together, these studies and the experiments performed in this thesis suggest nidogen plays an integral role in BM stability and therefore may be a key element in its disassembly.

Laminin zebrafish mutants display similar phenotypes to nidogen morphants

In addition to studies of *nidogen* mutants, there have been reports showing the ablation of other basement membrane components resulting in adverse effects on ocular development with similar phenotypes to those observed in nidogen morphant embryos. For example, loss of *laminina1* has been observed to effect zebrafish vertebrate optic cup

morphogenesis (Bryan et al. 2016). The authors were able to determine multiple structural abnormalities in zebrafish embryos lacking laminin *α1* including defects in focal adhesion, invagination, and optic stalk constriction. On a macroscopic level they observed morphogenic phenotypes similar to nidogen morphants including a misshapen lens, and smaller eyes (Fig. 17). The authors also noted patches of dying cells they hypothesized could be a result of cells losing contact with the basement membrane and entering into apoptosis via anoikis. Similarly, in my live imaging study of nidogen morphants, I observed cells which had seemingly lost contact with the basement membrane and were subsequently detached from the eye (Fig. 19).

An additional study observing mutants for both *laminin β1* and *laminin γ1* showed basement membrane defects effecting both the developing eye and notochord of zebrafish (Parsons et al. 2002). Both mutants showed smaller eyes and lens abnormalities similar to those observed in nidogen morphants and dominant negative nidogen embryos (Fig. 17 and Fig.22). Furthermore, these embryos also displayed shortened body axis comparable to nidogen morphant embryos. Together these studies suggest BM integrity is essential to proper embryonic development and that loss of even one component can robustly alter morphogenesis.

How nidogen removal can alter basement membrane dynamics prior to ESF

Although limiting or removing nidogen results in destabilized BM structure the question remains however how nidogen removal may initiate disruption of BM integrity ultimately leading to BM removal and subsequent ESF. I hypothesize that there are two potential modes in which the structural disassembly of the BM through the removal of nidogen is necessary for ESF to occur. The first predicts that the removal of nidogen from the BM results in the exposure of proteolytic sites in the core BM components of laminin, collagenIV or perlecan. Specifically, nidogens removal leads to a disrupted basement membrane architecture allowing for the subsequent liberation of newly exposed epitopes in other basement membrane components. In this model, matrix metalloproteases which recognize these newly exposed epitopes now have the ability to efficiently remodel

basement membrane components leading to the efficient breakdown of the BM allowing subsequent ESF.

The second mode predicts that in the absence of nidogen, BM integrity is compromised allowing for the extension of cellular protrusions required for ESF. Ultimately, reducing the biomechanical strength of the BM allows for the necessary positioning of epithelial sheets. It is not only possible, but likely, that these two proposed modes work in concert to enable fusion. In my thesis I have provided evidence that the regulation of nidogen within the choroid fissure may be a result of both expression dynamics and potentially targeted nidogen removal.

Regulation of nidogen and subsequent BM remodeling as a result of expression dynamics

Comparative gene expression analysis of all major BM components in the CF prior to and during ESF indicates that *nidogen* is first to be down regulated. Specifically, of the 10 genes examined to be expressed within the choroid fissure, *nidogen1a* and *2a* mRNA becomes undetectable earlier than *perlecan*, both *collagenIVs* (*4a1* and *4a2*), and two of the three *laminins* (*a1* and *c1*) (Table. 3) (Figs. 8-12). The question remains however, if the differential expression of BM components results in structural consequences that may ultimately prime the BM for remodeling.

An examination of other BM remodeling events provides evidence that gene expression does have the ability to play consequential roles in altering BM structure. During heart failure for example, the myocardial BM is significantly remodeled which has been hypothesized to alter cellular shape and function ultimately resulting in decreased performance (Kim et al. 2016). A study examining the variance of gene expression of ischemic failing and non-failing hearts in human tissue suggests that the differential expression of BM components, including the down-regulation of *nidogen* and *laminin*, do indeed effect BM morphology (Kim et al. 2016). Transmission electron microscopy revealed, amorphous disrupted BMs in failing hearts with lower levels of *nidogen* and *laminin* gene expression. Our results suggest, that the integrity of the BM of

the CF may decrease via a similar *developmental* mechanism in which the expression of *nidogen* is purposely reduced.

In addition to pathogenic instances, the genetic regulation of *nidogen* and *laminin* during development has also been shown to play a role in BM morphology. In the developing mouse lung, the differential spatial expression of *laminin* and its interaction with *nidogen* is thought to alter BM structure which ultimately facilitates branching morphogenesis (Thomas and Dziadek 1993). In this system, *nidogen* is expressed evenly throughout the developing lung tissue however *laminin* expression is spatially confined to the tips and base of the developing lobules. Laminin-nidogen complexes at the distal lobules and base of the branching lung thereby generate highly stabilized BM and regions between are thought to be discontinuous and thin. They hypothesize that lack of these complexes and subsequent weakening of the BM in the proliferating intermediate regions allows for the outgrowth and branching of the developing lung. Likewise, our data suggests that in the CF the expression of both *laminin* and *nidogen* decrease prior to that of *collagenIV* and *perlecan* which may ultimately effect BM architecture. This reduction of newly synthesized laminin-nidogen complexes, like in the developing mouse lung, may lead to thinner, more discontinuous BMs which can be more efficiently remodeled.

Protein level regulation of nidogen and subsequent BM remodeling

Although genetic regulation of *nidogen* and its interacting components likely play a role in the destabilization of the BM, direct targeting *nidogen* for removal from the BM on a protein level likely also affects BM stability. The morpholino analysis conducted in this study, knocking down the expression of *nidogen1a* and *1b*, resulted in observable alterations in BM integrity and robust morphological consequences (Figs. 16, 17, 18, and 19). Specifically, the morphology of *nidogen* morphant eyes were both significantly smaller and more elongated compared to controls. These changes in eye shape and size may be a result of a reduction of the biomechanical strength of BMs deficient for *nidogen* and subsequent failure of the BM to support the developing eye tissue.

It is important to note that since the completion of this study there has been an update of splice variants of the *nidogen1b* transcript in the zebrafish transcriptome. As reported by the Zebrafish Information Network (ZFIN) and Ensemble there are now 5 described splice variants of the *nidogen1b* gene. In this study, targeted silencing was conducted for the transcript variant nid1b-202 (ENSDARG00000103129) which codes for a protein 87 amino acids smaller than the largest variant (nid1b-201). Although the *nidogen1b* morpholino utilized in this study technically only targets the nid1b-202 splice variant, we are confident that there was a disruption of *nidogen1b* gene function which was responsible for the results observed. For example, phenotypic responses to *nidogen1a* and *1b* morpholinos independently were highly similar and when used together resulted in more robust aberrations (Fig. 16). Furthermore, inhibiting *nidogen1b* function via the use of dominant negative constructs phenocopied the morpholino associated gross morphological alterations in development strengthening our previous results.

The functional studies conducted in this thesis suggest BMs lacking *nidogen* are mechanically less stable and result in the impaired development of epithelial tissues. As such, endogenous targeting and removal of *nidogen* in the CF via endogenous proteases provides a likely route for dismantling the BM. Further, as the most proteolytically sensitive BM component, *nidogen* (Mayer et al. 1993/1994, Sires et al. 1993) is uniquely capable of acting as a lynchpin whereas its removal would directly result in the BM phenotypes observed in this study.

Further, it is predicted that the remodeling of the BM prior to fusion requires an assemblage of proteases capable of degrading matrix components found within this interstitial space. To date, several BM remodeling protease families have been discovered and characterized including, MMPs (Matrix metalloproteinases), ADAMs (a disintegrin and metalloproteinases), ADAMTSs (ADAMs with a thrombospondin motif), Meprins, and Cathepsins (Bonnans et al. 2014). Appropriate regulation of proteases has been shown to moderate BM remodeling and dysregulation has been observed to induce or accelerate numerous pathologies (Bondenson et al. 2008 and Daley et al. 2013).

One particular family of interest are the MMPs which are considered to be the primary enzymes involved in BM degradation, and collectively have the ability to target

all major BM components (Bonnans et al. 2014). To this point, MMPs have been implicated in BM remodeling during mammary epithelial branching and have been shown to play a key role in remodeling of intestinal BM (Zhang et al. 2013, and Fujimoto et al. 2007). Additionally, although broad in their targeting abilities, both *in vivo* and *in vitro* studies have provided evidence some MMPs specifically target nidogen (Tonge et al. 2013, Titz et al. 2004 and Alexander et al. 1996). Examined together, these data suggest MMPs may play a critical role in targeting nidogen for remodeling the BM of the CF and should be further examined.

Nidogen as a potential regulator of the biomechanical strength of basement membranes and epithelial fusion

One major hallmark of epithelial sheet fusion is the mechanical movement of opposing epithelia into juxtaposition. This migratory behavior is, at least in part, the result of actin based cellular protrusions called lamellipodia and filopodia. Cellular protrusions have been indicated in several epithelial fusion events across species including, dorsal closure in *Drosophila*, and neural tube closure in mice (Millard et al. 2008, Geelan et al. 1976). However cellular movement is achieved, it is clear that the persistence of an impassible BM would hinder or even halt migration leading to a failure of fusion. To overcome this, the embryo must remodel or eliminate this structural barrier possibly through the removal of nidogen to decrease tension and allow for movement.

Previous work has shown that altering the stoichiometry of BM components, specifically laminin-nidogen complexes results in weakening of the BM allowing for epithelial protrusion in the form of branching in the developing mouse lung (Thomas and Dziadek 1993). Additionally, interfering with laminin and nidogen interaction has also been shown to inhibit proper branching morphology of the submandibular gland in mice (Kadoya et al 1997). Examined together, these data suggest that BM integrity and strength may play a central role in epithelia movement and malleability. The data provided in this thesis suggests that inhibiting integration of nidogen results in a less uniform and more irregular deposition of BMs. Thereby, nidogen's removal may be a key

factor in reducing BM strength and allowing for the projection of epithelial protrusions and subsequent ESF in the CF.

Future Directions

I have provided evidence in this thesis that suggests that nidogen may be a potential regulator of BM disassembly prior to ESF however much remains to be discovered in relation to this hypothesis. Perhaps the most insightful experiment to be conducted is to establish a timeline of breakdown of all major BM components in the choroid fissure via IHC. Preliminary data generated in this thesis has identified the deposition of both nidogen and collagenIV in the choroid fissure at 24 and 48hpf. By expanding this data set to include both laminin and perlecan deposition throughout the entirety of the fusion processes a complete chronology of the breakdown of all components can be generated. If the hypothesis that nidogen acts as lynchpin for basement membrane disassembly proves correct, I would expect that nidogen's protein levels within the CF would diminish prior to that of its interacting components. This would support the premise that removal of nidogen may act a catalyst for BM breakdown via nidogen specific proteolytic targeting.

Further, future experiments conducted using dominant negative nidogen1b transgenic embryos will shed light on nidogens role in BM integrity and ESF in a more targeted context. The functional studies conducted in this thesis have examined the consequences of ubiquitous *nidogen* knockdown or introduction of dominant negative nidogen beginning at the one cell stage. Although both experiments resulted in basement membrane defects which lead to subsequent eye abnormalities, these experimental approaches are notably imperfect due to their ubiquitous nature. Because of this, it is impossible to determine if the observed eye phenotypes are a consequence of the loss of nidogen specifically in the eye. In fact, it likely that phenotypes observed in the eyes of nidogen morphants are a result of earlier developmental mechanisms reliant on nidogen deposition. Using the heatshock promoter to drive the expression of dominant negative nidogen1b later in development will circumvent some of these issues. For example, by

inhibiting nidogen's function prior to BM breakdown in the CF it may be possible to observe a premature dismantling of BM as a result of weakened ternary structure. This experiment would allow for the observation of impaired nidogen function in an embryo with no prior *nidogen* knockdown.

Additionally, it would be interesting to examine the biomechanical dynamics of the BM in the choroid fissure in both WT and nidogen morphants. Although elimination of nidogen from the BM in both mice and zebrafish has resulted in disrupted BMs, a direct measurement of the BM strength of tissues undergoing naturally remodeling has never been attempted. Likewise, a measurement of the strength of BMs lacking nidogen has yet to be acquired. Measurements of BM strength can be conducted utilizing atomic force microscopy (AFM). In fact, AFM has proven to be a useful tool for providing insight into the structural specifications and macromolecular organization of BMs in multiple studies (Chen and Handsma 2000, Last et al. 2009, and Mestres et al. 2014). Analyzing the biomechanical strength in BMs lacking nidogen may provide evidence that nidogen is a key regulator of BM integrity. Additionally, measuring the biomechanics of the BM of the choroid fissure throughout the process of fusion, together with the data generated in this study, may provide evidence that *nidogen* expression and deposition is a key regulator of BM strength. If true, these data would further support the hypothesis that the regulation of nidogen is necessary for the dismantling of the BM and subsequent fusion.

Conclusion

Ultimately the data generated from this study provides evidence that nidogen's crosslinking ability plays a key role in the stability of the BM of the CF and therefore may regulate its disassembly prior to ESF. An expression analysis of *nidogen* suggests it's downregulation precedes that of its interacting components in the CF thereby potentially priming the BM for removal. Additionally, a functional analysis of nidogen via morpholino mediated knockdown and dominant negative interference results in BM abnormalities, significant changes in eye size and shape, and altered gene expression of

eye patterning genes confirming its architectural importance. Together, these data provide the basis for a developmental mechanism in which nidogen acts as a lynchpin for BM stability and is thereby removed in anticipation of ESF.

Notably, the mechanisms of epithelial sheet fusion are thought to be conserved in many developing tissues. Therefore, it is also likely that the regulation of nidogen may play a key role in the BM remodeling mechanisms of other fusing tissues in both developing and adult tissues. Thus, the data presented in this thesis will provide valuable insight into other critical fusion events and ultimately into fusion derived diseases such as those described in CHARGE syndrome.

References

- Alexander, C.M., Howard, E.W., Bissell, M.J., Werb, Z., 1996. Rescue of mammary epithelial cell apoptosis and entactin degradation by a tissue inhibitor of metalloproteinases-1 transgene. *Journal of Cell Biology* 135, 1669-1677.
- Amsterdam, A., Hopkins, N., 2006. Mutagenesis strategies in zebrafish for identifying genes involved in development and disease. *Trends in Genetics* 22, 473-478.
- Aumailley, M., Wiedemann, H., Mann, K., Timpl, R., 1989. BINDING OF NIDOGEN AND THE LAMININ-NIDOGEN COMPLEX TO BASEMENT-MEMBRANE COLLAGEN TYPE-IV. *European Journal of Biochemistry* 184, 241-248.
- Bader, B.L., Smyth, N., Nedbal, S., Miosge, N., Baranowsky, A., Mokkapati, S., Murshed, M., Nischt, R., 2005. Compound genetic ablation of nidogen 1 and 2 causes basement membrane defects and perinatal lethality in mice. *Molecular and Cellular Biology* 25, 6846-6856.
- Baranowsky, A., Mokkapati, S., Bechtel, M., Krugel, J., Miosge, N., Wickenhauser, C., Smyth, N., Nischt, R., 2010. Impaired wound healing in mice lacking the basement membrane protein nidogen 1. *Matrix Biology* 29, 15-21.
- Barbieri, A., Alfano, G., Broccoli, V., Bulfone, A., Marigo, V., Bovolenta, P., Ballabio, A., Banfi, S., 2002. Vax2 inactivation in mouse determines alteration of the eye dorsal-ventral axis, misrouting of the optic fibers and eye coloboma. *European Journal of Human Genetics* 10, 235-235.
- Bibliowicz, J., Tittle, R.K., Gross, J.M., 2011. Toward a Better Understanding of Human Eye Disease: Insights From the Zebrafish, *Danio rerio*, in: Chang, K.T., Min, K.T. (Eds.), *Animal Models of Human Disease*. Elsevier Academic Press Inc, San Diego, pp. 287-330.
- Bohnsack, B.L., Kasprick, D.S., Kish, P.E., Goldman, D., Kahana, A., 2012. A Zebrafish Model of Axenfeld-Rieger Syndrome Reveals That pitx2 Regulation by Retinoic Acid Is Essential for Ocular and Craniofacial Development. *Investigative Ophthalmology & Visual Science* 53, 7-22.
- Bondeson, J., Wainwright, S., Hughes, C., Caterson, B., 2008. The regulation of the ADAMTS4 and ADAMTS5 aggrecanases in osteoarthritis: a review. *Clinical and Experimental Rheumatology* 26, 139-145.
- Bose, K., Nischt, R., Page, A., Bader, B.L., Paulsson, M., Smyth, N., 2006. Loss of nidogen-1 and-2 results in syndactyly and changes in limb development. *Journal of Biological Chemistry* 281, 39620-39629.

- Bower, M., Salomon, R., Allanson, J., Antignac, C., Benedicenti, F., Benetti, E., Binenbaum, G., Jensen, U.B., Cochat, P., DeCramer, S., Dixon, J., Drouin, R., Falk, M.J., Feret, H., Gise, R., Hunter, A., Johnson, K., Kumar, R., Lavocat, M.P., Martin, L., Moriniere, V., Mowat, D., Murer, L., Nguyen, H.T., Peretz-Amit, G., Pierce, E., Place, E., Rodig, N., Salerno, A., Sastry, S., Sato, T., Sayer, J.A., Schaafsma, G.C.P., Shoemaker, L., Stockton, D.W., Tan, W.H., Tenconi, R., Vanhille, P., Vats, A., Wang, X.J., Warman, B., Weleber, R.G., White, S.M., Wilson-Brackett, C., Zand, D.J., Eccles, M., Schimmenti, L.A., Heidet, L., 2012. Update of PAX2 mutations in renal coloboma syndrome and establishment of a locus-specific database. *Human Mutation* 33, 457-466.
- Bryan, C.D., Chien, C.B., Kwan, K.M., 2016. Loss of laminin alpha 1 results in multiple structural defects and divergent effects on adhesion during vertebrate optic cup morphogenesis. *Developmental Biology* 416, 324-337.
- Burmeister, M., Novak, T., Liang, M.Y., Basu, S., Ploder, L., Hawes, N.L., Vidgen, D., Hoover, F., Goldman, D., Kalnins, V.I., Roderick, T.H., Taylor, B.A., Hankin, M.H., McInnes, R.R., 1996. Ocular retardation mouse caused by Chx10 homeobox null allele: Impaired retinal progenitor proliferation and bipolar cell differentiation. *Nature Genetics* 12, 376-384.
- Cai, Z.G., Tao, C.Q., Li, H.G., Ladher, R., Gotoh, N., Feng, G.S., Wang, F., Zhang, X., 2013. Deficient FGF signaling causes optic nerve dysgenesis and ocular coloboma. *Development* 140, 2711-2723.
- Candiello, J., Balasubramani, M., Schreiber, E.M., Cole, G.J., Mayer, U., Halfter, W., Lin, H., 2007. Biomechanical properties of native basement membranes. *Febs Journal* 274, 2897-2908.
- Cepko, C.L., Austin, C.P., Yang, X.J., Alexiades, M., 1996. Cell fate determination in the vertebrate retina. *Proceedings of the National Academy of Sciences of the United States of America* 93, 589-595.
- Chang, L., Blain, D., Bertuzzi, S., Brooks, B.P., 2006. Uveal coloboma: clinical and basic science update. *Current Opinion in Ophthalmology* 17, 447-470.
- Chen, C.H., Hansma, H.G., 2000. Basement membrane macromolecules: Insights from atomic force microscopy. *Journal of Structural Biology* 131, 44-55.
- Chiang, C., Ying, L.T.T., Lee, E., Young, K.E., Corden, J.L., Westphal, H., Beachy, P.A., 1996. Cyclopia and defective axial patterning in mice lacking Sonic hedgehog gene function. *Nature* 383, 407-413.

- Creuzet, S., Vincent, C., Couly, G.R., 2005. Neural crest derivatives in ocular and periocular structures. *International Journal of Developmental Biology* 49, 161-171.
- Daley, W.P., Yamada, K.M., 2013. ECM-modulated cellular dynamics as a driving force for tissue morphogenesis. *Current Opinion in Genetics & Development* 23, 408-414.
- Dutton, K.A., Pauliny, A., Lopes, S.S., Elworthy, S., Carney, T.J., Rauch, J., Geisler, R., Haffter, P., Kelsh, R.N., 2001. Zebrafish colourless encodes sox10 and specifies non-ectomesenchymal neural crest fates. *Development* 128, 4113-4125.
- Dziadek, M., Mitrangas, K., 1989. DIFFERENCES IN THE SOLUBILITY AND SUSCEPTIBILITY TO PROTEOLYTIC DEGRADATION OF BASEMENT-MEMBRANE COMPONENTS IN ADULT AND EMBRYONIC MOUSE-TISSUES. *American Journal of Anatomy* 184, 298-310.
- Easter, S.S., Nicola, G.N., 1995. THE DEVELOPMENT OF VISION AND EYE-MOVEMENTS IN ZEBRAFISH (DANIO-RERIO). *Investigative Ophthalmology & Visual Science* 36, S762-S762.
- Ekker, S.C., Ungar, A.R., Greenstein, P., Vonkessler, D.P., Porter, J.A., Moon, R.T., Beachy, P.A., 1995. PATTERNING ACTIVITIES OF VERTEBRATE HEDGEHOG PROTEINS IN THE DEVELOPING EYE AND BRAIN. *Current Biology* 5, 944-955.
- Fadool, J.M., Dowling, J.E., 2008. Zebrafish: A model system for the study of eye genetics. *Progress in Retinal and Eye Research* 27, 89-110.
- Fata, J.E., Werb, Z., Bissell, M.J., 2004. Regulation of mammary gland branching morphogenesis by the extracellular matrix and its remodeling enzymes. *Breast Cancer Research* 6, 1-11.
- Favor, J., Gloeckner, C.J., Neuhauser-Klaus, A., Pretsch, W., Sandulache, R., Saule, S., Zaus, I., 2008. Relationship of Pax6 activity levels to the extent of eye development in the mouse, *Mus musculus*. *Genetics* 179, 1345-1355.
- Favor, J., Sandulache, R., NeuhauserKlaus, A., Pretsch, W., Chatterjee, B., Senft, E., Wurst, W., Blanquet, V., Grimes, P., Sporle, R., Schughart, K., 1996. The mouse Pax2(1Neu) mutation is identical to a human PAX2 mutation in a family with renal-coloboma syndrome and results in developmental defects of the brain, ear, eye, and kidney. *Proceedings of the National Academy of Sciences of the United States of America* 93, 13870-13875.

- Feitosa, N.M., Richardson, R., Bloch, W., Hammerschmidt, M., 2011. Basement Membrane Diseases in Zebrafish, in: Detrich, H.W., Westerfield, M., Zon, L.I. (Eds.), *Zebrafish: Disease Models and Chemical Screens*, 3rd Edition. Elsevier Academic Press Inc, San Diego, pp. 191-222.
- FitzPatrick, D.R., van Heyningen, V., 2005. Developmental eye disorders. *Current Opinion in Genetics & Development* 15, 348-353.
- Fuhrmann, S., 2010. EYE MORPHOGENESIS AND PATTERNING OF THE OPTIC VESICLE, in: Cagan, R.L., Reh, T.A. (Eds.), *Invertebrate and Vertebrate Eye Development*. Elsevier Academic Press Inc, San Diego, pp. 61-84.
- Gage, P.J., Rhoades, W., Prucka, S.K., Hjalt, T., 2005. Fate maps of neural crest and mesoderm in the mammalian eye. *Investigative Ophthalmology & Visual Science* 46, 4200-4208.
- Geelen, J.A.G., Langman, J., 1979. ULTRASTRUCTURAL OBSERVATIONS ON CLOSURE OF THE NEURAL TUBE IN THE MOUSE. *Anatomy and Embryology* 156, 73-88.
- Graw, J., 1996. Genetic aspects of embryonic eye development in vertebrates. *Developmental Genetics* 18, 181-197.
- Gregory-Evans, C.Y., Williams, M.J., Halford, S., Gregory-Evans, K., 2004. Ocular coloboma: a reassessment in the age of molecular neuroscience. *Journal of Medical Genetics* 41, 881-891.
- Guercio, J.R., Martyn, L.J., 2007. Congenital malformations of the eye and orbit. *Otolaryngologic Clinics of North America* 40, 113-+.
- Hartsock, A., Lee, C., Arnold, V., Gross, J.M., 2014. In vivo analysis of hyaloid vasculature morphogenesis in zebrafish: A role for the lens in maturation and maintenance of the hyaloid. *Developmental Biology* 394, 327-339.
- Heavner, W., Pevny, L., 2012. *Eye Development and Retinogenesis*. Cold Spring Harbor Perspectives in Biology 4.
- Hero, I., 1990. OPTIC FISSURE CLOSURE IN THE NORMAL CINNAMON MOUSE - AN ULTRASTRUCTURAL-STUDY. *Investigative Ophthalmology & Visual Science* 31, 197-216.
- Holmberg, J., Clarke, D.L., Frisen, J., 2000. Regulation of repulsion versus adhesion by different splice forms of an Eph receptor. *Nature* 408, 203-206.

- Horsford, D.J., Nguyen, M.T.T., Sellar, G.C., Kothary, R., Arnheiter, H., McInnes, R.R., 2005. Chx10 repression of Mitf is required for the maintenance of mammalian neuroretinal identity. *Development* 132, 177-187.
- Hurd, E.A., Capers, P.L., Blauwkamp, M.N., Adams, M.E., Raphael, Y., Poucher, H.K., Martin, D.M., 2007. Loss of Chd7 function in gene-trapped reporter mice is embryonic lethal and associated with severe defects in multiple developing tissues. *Mammalian Genome* 18, 94-104.
- Hutter, H., Vogel, B.E., Plenefisch, J.D., Norris, C.R., Proenca, R.B., Spieth, J., Guo, C.B., Mastwal, S., Zhu, X.P., Scheel, J., Hedgecock, E.M., 2000. Cell biology: Conservation and novelty in the evolution of cell adhesion and extracellular matrix genes. *Science* 287, 989-994.
- Hynes, R.O., 2012. The evolution of metazoan extracellular matrix. *Journal of Cell Biology* 196, 671-679.
- Hynes, R.O., Zhao, Q., 2000. The evolution of cell adhesion. *Journal of Cell Biology* 150, F89-F95.
- Ivanovitch, K., Cavodeassi, F., Wilson, S.W., 2013. Precocious Acquisition of Neuroepithelial Character in the Eye Field Underlies the Onset of Eye Morphogenesis. *Developmental Cell* 27, 293-305.
- Jacinto, A., Martinez-Arias, A., Martin, P., 2001. Mechanisms of epithelial fusion and repair. *Nature Cell Biology* 3, E117-E123.
- James, A., Lee, C., Williams, A.M., Angileri, K., Lathrop, K.L., Gross, J.M., 2016. The hyaloid vasculature facilitates basement membrane breakdown during choroid fissure closure in the zebrafish eye. *Developmental Biology* 419, 262-272.
- Kadoya, Y., Salmivirta, K., Talts, J.F., Kadoya, K., Mayer, U., Timpl, R., Ekblom, P., 1997. Importance of nidogen binding to laminin gamma 1 for branching epithelial morphogenesis of the submandibular gland. *Development* 124, 683-691.
- Kim, E.H., Galchev, V.I., Kim, J.Y., Misek, S.A., Stevenson, T.K., Campbell, M.D., Pagani, F.D., Day, S.M., Johnson, T.C., Washburn, J.G., Vikstrom, K.L., Michele, D.E., Misek, D.E., Westfall, M.V., 2016. Differential protein expression and basal lamina remodeling in human heart failure. *Proteomics Clinical Applications* 10, 585-596.
- Knickmeyer, M.D., Mateo, J.L., Eckert, P., Roussa, E., Rahhal, B., Zuniga, A., Kriegelstein, K., Wittbrodt, J., Heermann, S., 2018. TGF beta-facilitated optic

- fissure fusion and the role of bone morphogenetic protein antagonism. *Open Biology* 8, 13.
- Kwan, K.M., Fujimoto, E., Grabher, C., Mangum, B.D., Hardy, M.E., Campbell, D.S., Parant, J.M., Yost, H.J., Kanki, J.P., Chien, C.B., 2007. The Tol2kit: A multisite Gateway-based construction kit for Tol2 transposon transgenesis constructs. *Developmental Dynamics* 236, 3088-3099.
- Lang, R.A., 2004. Pathways regulating lens induction in the mouse. *International Journal of Developmental Biology* 48, 783-791.
- Last, J.A., Liliensiek, S.J., Nealey, P.F., Murphy, C.J., 2009. Determining the mechanical properties of human corneal basement membranes with atomic force microscopy. *Journal of Structural Biology* 167, 19-24.
- Li, S.H., Edgar, D., Fassler, R., Wadsworth, W., Yurchenco, P.D., 2003. The role of laminin in embryonic cell polarization and tissue organization. *Developmental Cell* 4, 613-624.
- Li, Z., Joseph, N.M., Easter, S.S., 2000. The morphogenesis of the zebrafish eye, including a fate map of the optic vesicle. *Developmental Dynamics* 218, 175-188.
- Little, S.C., Mullins, M.C., 2005. Twisted gastrulation promotes BMP signaling in zebrafish DV axial patterning. *Developmental Biology* 283, 620-620.
- Liu, C.Q., Widen, S.A., Williamson, K.A., Ratnapriya, R., Gerth-Kahlert, C., Rainger, J., Alur, R.P., Strachan, E., Manjunath, S.H., Balakrishnan, A., Floyd, J.A., Li, T.S., Waskiewicz, A., Brooks, B.P., Lehmann, O.J., FitzPatrick, D.R., Swaroop, A., Consortium, U.K., 2016. A secreted WNT-ligand-binding domain of FZD5 generated by a frameshift mutation causes autosomal dominant coloboma. *Human Molecular Genetics* 25, 1382-1391.
- Loosli, F., Staub, W., Finger-Baier, K.C., Ober, E.A., Verkade, H., Wittbrodt, J., Baier, H., 2003. Loss of eyes in zebrafish caused by mutation of *chokh/rx3*. *Embo Reports* 4, 894-899.
- Macdonald, A.E., 1965. CAUSES OF BLINDNESS IN CANADA - AN ANALYSIS OF 24605 CASES REGISTERED WITH CANADIAN NATIONAL INSTITUTE FOR BLIND. *Canadian Medical Association Journal* 92, 264-+.
- Masland, R.H., 2012. The Neuronal Organization of the Retina. *Neuron* 76, 266-280.
- Mathers, P.H., Grinberg, A., Mahon, K.A., Jamrich, M., 1997. The *Rx* homeobox gene is essential for vertebrate eye development. *Nature* 387, 603-607.

- Matt, N., Ghyselinck, N.B., Pellerin, I., Dupe, V., 2008. Impairing retinoic acid signalling in the neural crest cells is sufficient to alter entire eye morphogenesis. *Developmental Biology* 320, 140-148.
- Mayer, U., Mann, K., Timpl, R., Murphy, G., 1993. SITES OF NIDOGEN CLEAVAGE BY PROTEASES INVOLVED IN TISSUE HOMEOSTASIS AND REMODELING. *European Journal of Biochemistry* 217, 877-884.
- Mayer, U., Zimmermann, K., Mann, K., Reinhardt, D., Timpl, R., Nischt, R., 1995. BINDING-PROPERTIES AND PROTEASE STABILITY OF RECOMBINANT HUMAN NIDOGEN. *European Journal of Biochemistry* 227, 681-686.
- McMahon, C., Gestri, G., Wilson, S.W., Link, B.A., 2009. Lmx1b is essential for survival of periocular mesenchymal cells and influences Fgf-mediated retinal patterning in zebrafish. *Developmental Biology* 332, 287-298.
- Mestres, P., Gomez, L.L., Lopez, T.N., del Rosario, G., Lukas, S.W., Hartmann, U., 2014. The basement membrane of the isolated rat colonic mucosa. A light, electron and atomic force microscopy study. *Annals of Anatomy-Anatomischer Anzeiger* 196, 108-118.
- Millard, T.H., Martin, P., 2008. Dynamic analysis of filopodial interactions during the zippering phase of *Drosophila* dorsal closure. *Development* 135, 621-626.
- Millicovsky, G., Johnston, M.C., 1981. ACTIVE-ROLE OF EMBRYONIC FACIAL EPITHELIUM - NEW EVIDENCE OF CELLULAR EVENTS IN MORPHOGENESIS. *Journal of Embryology and Experimental Morphology* 63, 53-66.
- Morris, A.C., 2011. The Genetics of Ocular Disorders: Insights From The Zebrafish. *Birth Defects Research Part C-Embryo Today-Reviews* 93, 215-228.
- Murai, K.K., Pasquale, E.B., 2003. 'Eph'ective signaling: forward, reverse and crosstalk. *Journal of Cell Science* 116, 2823-2832.
- Nguyen, M.T.T., Arnheiter, H., 2000a. Signaling and transcriptional regulation in early mammalian eye development: a link between FGF and MITF. *Development* 127, 3581-3591.
- Nguyen, M.T.T., Arnheiter, H., 2000b. Signaling and transcriptional regulation in early mammalian eye development: a link between FGF and MITF. *Development* 127, 3581-3591.

- Nornes, H.O., Dressler, G.R., Knapik, E.W., Deutsch, U., Gruss, P., 1990. SPATIALLY AND TEMPORALLY RESTRICTED EXPRESSION OF PAX2 DURING MURINE NEUROGENESIS. *Development* 109, 797-809.
- Ogino, H., Ochi, H., Reza, H.M., Yasuda, K., 2012. Transcription factors involved in lens development from the preplacodal ectoderm. *Developmental Biology* 363, 333-347.
- Onwochei, B.C., Simon, J.W., Bateman, J.B., Couture, K.C., Mir, E., 2000a. Ocular colobomata. *Survey of Ophthalmology* 45, 175-194.
- Onwochei, B.C., Simon, J.W., Bateman, J.B., Couture, K.C., Mir, E., 2000b. Ocular colobomata. *Survey of Ophthalmology* 45, 175-194.
- Orioli, D., Henkemeyer, M., Lemke, G., Klein, R., Pawson, T., 1996. Sek4 and Nuk receptors cooperate in guidance of commissural axons and in palate formation. *Embo Journal* 15, 6035-6049.
- Page-McCaw, A., Serano, J., Sante, J.M., Rubin, G.M., 2003. Drosophila matrix metalloproteinases are required for tissue remodeling, but not embryonic development. *Developmental Cell* 4, 95-106.
- Pai, Y.J., Abdullah, N.L., Mohd-Zin, S.W., Mohammed, R.S., Rolo, A., Greene, N.D.E., Abdul-Aziz, N.M., Copp, A.J., 2012. Epithelial fusion during neural tube morphogenesis. *Birth Defects Research Part a-Clinical and Molecular Teratology* 94, 817-823.
- Parsons, M.J., Pollard, S.M., Saude, L., Feldman, B., Coutinho, P., Hirst, E.M.A., Stemple, D.L., 2002. Zebrafish mutants identify an essential role for laminins in notochord formation. *Development* 129, 3137-3146.
- Paulsson, M., Yurchenco, P.D., Ruben, G.C., Engel, J., Timpl, R., 1987. STRUCTURE OF LOW-DENSITY HEPARAN-SULFATE PROTEOGLYCAN ISOLATED FROM A MOUSE-TUMOR BASEMENT-MEMBRANE. *Journal of Molecular Biology* 197, 297-313.
- Pillai-Kastoori, L., Wen, W., Wilson, S.G., Strachan, E., Lo-Castro, A., Fichera, M., Musumeci, S.A., Lehmann, O.J., Morris, A.C., 2014. Sox11 Is Required to Maintain Proper Levels of Hedgehog Signaling during Vertebrate Ocular Morphogenesis. *Plos Genetics* 10, 19.
- Prada, C., Puga, J., Perezmendez, L., Lopez, R., Ramirez, G., 1991. SPATIAL AND TEMPORAL PATTERNS OF NEUROGENESIS IN THE CHICK RETINA. *European Journal of Neuroscience* 3, 559-569.

- Rahhal, B., Heermann, S., Ferdinand, A., Rosenbusch, J., Rickmann, M., Krieglstein, K., 2009. In vivo requirement of TGF-beta/GDNF cooperativity in mouse development: focus on the neurotrophic hypothesis. *International Journal of Developmental Neuroscience* 27, 97-102.
- Rao, M.B., Didiano, D., Patton, J.G., 2017. Neurotransmitter-Regulated Regeneration in the Zebrafish Retina. *Stem Cell Reports* 8, 831-842.
- Ray, H.J., Niswander, L., 2012. Mechanisms of tissue fusion during development. *Development* 139, 1701-1711.
- Rembold, M., Loosli, F., Adams, R.J., Wittbrodt, J., 2006. Individual cell migration serves as the driving force for optic vesicle evagination. *Science* 313, 1130-1134.
- Richardson, R., Tracey-White, D., Webster, A., Moosajee, M., 2017. The zebrafish eye-a paradigm for investigating human ocular genetics. *Eye* 31, 68-86.
- Rifat, Y., Parekh, V., Wilanowski, T., Hislop, N.R., Auden, A., Ting, S.B., Cunningham, J.M., Jane, S.M., 2010. Regional neural tube closure defined by the Grainy head-like transcription factors. *Developmental Biology* 345, 237-245.
- Russell, C., 2003. The roles of Hedgehogs and Fibroblast Growth Factors in eye development and retinal cell rescue. *Vision Research* 43, 899-912.
- Saint-Geniez, M., D'Amore, P.A., 2004. Development and pathology of the hyaloid, choroidal and retinal vasculature. *International Journal of Developmental Biology* 48, 1045-1058.
- Sanyanusin, P., Schimmenti, L.A., McNoe, L.A., Ward, T.A., Pierpont, M.E.M., Sullivan, M.J., Dobyms, W.B., Eccles, M.R., 1995. MUTATION OF THE PAX2 GENE IN A FAMILY WITH OPTIC-NERVE COLOBOMAS, RENAL ANOMALIES AND VESICOURETERAL REFLUX. *Nature Genetics* 9, 358-364.
- Sasagawa, S., Takabatake, T., Takabatake, Y., Muramatsu, T., Takeshima, K., 2002. Axes establishment during eye morphogenesis in *Xenopus* by coordinate and antagonistic actions of BMP4, Shh, and RA. *Genesis* 33, 86-96.
- Schimmenti, L.A., de la Cruz, J., Lewis, R.A., Karkera, J.D., Manligas, G.S., Roessler, E., Muenke, M., 2003. Novel mutation in sonic hedgehog in non-syndromic colobomatous microphthalmia. *American Journal of Medical Genetics Part A* 116A, 215-221.

- Schmitt, E.A., Dowling, J.E., 1994. EARLY EYE MORPHOGENESIS IN THE ZEBRAFISH, BRACHYDANIO-RERIO. *Journal of Comparative Neurology* 344, 532-542.
- Schmitt, E.A., Dowling, J.E., 1999. Early retinal development in the zebrafish, *Danio rerio*: Light and electron microscopic analyses. *Journal of Comparative Neurology* 404, 515-536.
- Schwarz, M., Cecconi, F., Bernier, G., Andrejewski, N., Kammandel, B., Wagner, M., Gruss, P., 2000. Spatial specification of mammalian eye territories by reciprocal transcriptional repression of Pax2 and Pax6. *Development* 127, 4325-4334.
- Seo, S., Chen, L.S., Liu, W.Z., Zhao, D.M., Schultz, K.M., Sasman, A., Liu, T., Zhang, H.F., Gage, P.J., Kume, T., 2017. Foxc1 and Foxc2 in the Neural Crest Are Required for Ocular Anterior Segment Development. *Investigative Ophthalmology & Visual Science* 58, 1368-1377.
- Shapiro, L., Fannon, A.M., Kwong, P.D., Thompson, A., Lehmann, M.S., Grubel, G., Legrand, J.F., Alsniesen, J., Colman, D.R., Hendrickson, W.A., 1995. STRUCTURAL BASIS OF CELL-CELL ADHESION BY CADHERINS. *Nature* 374, 327-337.
- Sires, U.I., Griffin, G.L., Broekelmann, T.J., Mecham, R.P., Murphy, G., Chung, A.E., Welgus, H.G., Senior, R.M., 1993. DEGRADATION OF ENTACTIN BY MATRIX METALLOPROTEINASES - SUSCEPTIBILITY TO MATRILYSIN AND IDENTIFICATION OF CLEAVAGE SITES. *Journal of Biological Chemistry* 268, 2069-2074.
- Smith, S.M.L., West, L.A., Govindraj, P., Zhang, X.Q., Ornitz, D.M., Hassell, J.R., 2007. Heparan and chondroitin sulfate on growth plate perlecan mediate binding and delivery of FGF-2 to FGF receptors. *Matrix Biology* 26, 175-184.
- Soules, K.A., Link, B.A., 2005. Morphogenesis of the anterior segment in the zebrafish eye. *Bmc Developmental Biology* 5.
- Stephen, L.J., Fawkes, A.L., Verhoeve, A., Lemke, G., Brown, A., 2007. A critical role for the EphA3 receptor tyrosine kinase in heart development. *Developmental Biology* 302, 66-79.
- Stoll, C., Alembik, Y., Dott, B., Roth, M.P., 1992. EPIDEMIOLOGY OF CONGENITAL EYE MALFORMATIONS IN 131,760 CONSECUTIVE BIRTHS. *Ophthalmic Paediatrics and Genetics* 13, 179-186.

- Svoboda, K.K.H., Oshea, K.S., 1987a. AN ANALYSIS OF CELL-SHAPE AND THE NEUROEPITHELIAL BASAL LAMINA DURING OPTIC VESICLE FORMATION IN THE MOUSE EMBRYO. *Development* 100, 185-200.
- Svoboda, K.K.H., Oshea, K.S., 1987b. AN ANALYSIS OF CELL-SHAPE AND THE NEUROEPITHELIAL BASAL LAMINA DURING OPTIC VESICLE FORMATION IN THE MOUSE EMBRYO. *Development* 100, 185-200.
- Take-uchi, M., Clarke, J.D.W., Wilson, S.W., 2003. Hedgehog signalling maintains the optic stalk-retinal interface through the regulation of Vax gene activity. *Development* 130, 955-968.
- Taya, Y., O'Kane, S., Ferguson, M.W.J., 1999. Pathogenesis of cleft palate in TGF-beta 3 knockout mice. *Development* 126, 3869-3879.
- Thomas, T., Dziadek, M., 1994. EXPRESSION OF COLLAGEN ALPHA-1(IV), LAMININ AND NIDOGEN GENES IN THE EMBRYONIC MOUSE LUNG - IMPLICATIONS FOR BRANCHING MORPHOGENESIS. *Mechanisms of Development* 45, 193-201.
- Timpl, R., 1993. PROTEOGLYCANS OF BASEMENT-MEMBRANES. *Experientia* 49, 417-428.
- Titz, B., Dietrich, S., Sadowski, T., Beck, C., Petersen, A., Sedlacek, R., 2004. Activity of MMP-19 inhibits capillary-like formation due to processing of nidogen-1. *Cellular and Molecular Life Sciences* 61, 1826-1833.
- Tonge, D., Zhu, N., Lynham, S., Leclere, P., Snape, A., Brewer, A., Schlomann, U., Ferdous, T., Tennyson, C., Bartsch, J.W., Ward, M., Pizzey, J., 2013. Axonal growth towards *Xenopus* skin in vitro is mediated by matrix metalloproteinase activity. *European Journal of Neuroscience* 37, 519-531.
- Torres, M.A., GomezPardo, E., Gruss, P., 1996. Pax2 contributes to inner ear patterning and optic nerve trajectory. *Development* 122, 3381-3391.
- Tryggvason, K., 1993. The laminin family. *Current Opinion in Cell Biology* 5, 877-882.
- Wen, W., Pillai-Kastoori, L., Wilson, S.G., Morris, A.C., 2015. Sox4 regulates choroid fissure closure by limiting Hedgehog signaling during ocular morphogenesis. *Developmental Biology* 399, 139-153.
- Werth, M., Walentin, K., Aue, A., Schonheit, J., Wuebken, A., Pode-Shakked, N., Vilianovitch, L., Erdmann, B., Dekel, B., Bader, M., Barasch, J., Rosenbauer, F., Luft, F.C., Schmidt-Ott, K.M., 2010. The transcription factor grainyhead-like 2 regulates the molecular composition of the epithelial apical junctional complex. *Development* 137, 3835-3845.

- Williamson, K.A., Rainger, J., Floyd, J.A.B., Ansari, M., Meynert, A., Aldridge, K.V., Rainger, J.K., Anderson, C.A., Moore, A.T., Hurles, M.E., Clarke, A., van Heyningen, V., Verloes, A., Taylor, M.S., Wilkie, A.O.M., FitzPatrick, D.R., Consortium, U.K., 2014. Heterozygous Loss-of-Function Mutations in YAP1 Cause Both Isolated and Syndromic Optic Fissure Closure Defects. *American Journal of Human Genetics* 94, 295-302.
- Woolner, S., Jacinto, A., Martin, P., 2005. The small GTPase Rac plays multiple roles in epithelial sheet fusion - Dynamic studies of *Drosophila* dorsal closure. *Developmental Biology* 282, 163-173.
- Wyatt, R.A., Keow, J.Y., Harris, N.D., Hache, C.A., Li, D.H., Crawford, B.D., 2009. The Zebrafish Embryo: A Powerful Model System for Investigating Matrix Remodeling. *Zebrafish* 6, 347-354.
- Yurchenco, P.D., Schittny, J.C., 1990. MOLECULAR ARCHITECTURE OF BASEMENT-MEMBRANES. *Faseb Journal* 4, 1577-1590.
- Zuber, M.E., Gestri, G., Viczian, A.S., Barsacchi, G., Harris, W.A., 2003. Specification of the vertebrate eye by a network of eye field transcription factors. *Development* 130, 5155-5167.

Vita

Nicholas Carrara

Education

B.S. in Biology, Longwood University, 2015

Professional Experience

- Graduate Research Assistant, University of Kentucky, *August, 2015-July, 2018*
- Graduate Teaching Assistant, University of Kentucky, *August, 2015-May, 2017*
- Undergraduate Research Assistant, Longwood University, *September 2013-May, 2015*

Scholastic and Professional Honors

- National Science Foundation Fellowship- Honorable Mention, *Spring, 2017*
- Student Scholarship for Outstanding Vision Research, Knights Templar Eye Foundation, *Spring, 2016*
- Most Outstanding Senior in Biological Sciences, Longwood University, *Spring, 2015*
- Best Biology Oral Presentation and Poster Presentation, Big South Research Conference, *Spring, 2015*
- Most Outstanding Junior in Biological sciences, Longwood University, *Spring, 2014*

Publications

- **Carrara, N., Settell, K., Andrews, B., Buckalew, D., and Znosko, W.** Expanding the Indicator Bacteria Concept: a Novel Approach to Assess Ecosystem Risk in Impaired Waters. **Journal of Water Resource and Protection.**

Nicholas William Carrara